Astronomy & Astrophysics manuscript no. MILONEetal October 16, 2008
(DOI: will be inserted by hand later)

arXiv:0810.2558v1 [astro-ph] 14 Oct 2008

Multiple stellar populations in Magellanic Clouds clusters. ⋆

I. An ordinary feature for intermediate age globulars in the LMC?

A. P. Milone[1], L. R. Bedin[2], G. Piotto[1], and J. Anderson[2]

[1] Dipartimento di Astronomia, Università di Padova, Vicolo dell'Osservatorio 3, Padova, I-35122, Italy
[2] Space Telescope Science Institute, 3700 San Martin Drive, Baltimore, MD 21218, USA

Received Xxxxx xx, xxxx; accepted Xxxx xx, xxxx

Abstract.
Context: The discovery of multiple main sequences (MS) in the massive clusters NGC 2808 and Omega Centauri, and multiple subgiant branches in NGC 1851 and NGC 6388 has challenged the long-held paradigm that globular clusters consist of simple stellar populations. This evolving picture has been further complicated by recent photometric studies of the Large Magellanic Cloud (LMC) intermediate-age clusters, where the main sequence turn-off (MSTO) was found to be bimodal (NGC 1806 and NGC 1846) or broadened (NGC 1783 and NGC 2173).
Aims: We have undertaken a study of archival *HST* images of Large and Small Magellanic Cloud clusters with the aim of measuring the frequency of clusters with evidence of multiple or prolonged star formation events and determining their main properties. We found useful images for 53 clusters that cover a wide range of ages. In this paper, we analyse the Color-Magnitude Diagrams (CMD) of sixteen intermediate-age (∼ 1-3 Gyr) LMC clusters.
Methods: The data were reduced by using the method developed by Anderson et al. (2008) and the photometry has been corrected for differential reddening (where required). We find that eleven clusters show an anomalous spread (or split) in color and magnitude around the MSTO, even though the other main features of the CMD (MS, red giant branch, asymptotic giant branch) are narrow and the horizontal branch (HB) red-clump well defined. By using the CMD of the stars in regions that surround the cluster, we demonstrate that the observed feature is unequivocally associated to the clusters. We use artificial-star tests to demonstrate that the spread (or split) is not an artifact due to photometric errors or binaries.
Results: We confirm that two clusters (NGC 1806 and NGC 1846) clearly exhibit two distinct MSTOs and observe, for the first time, a double MSTO in NGC 1751. In these three clusters the population corresponding to the brighter MSTO includes more than two-thirds of cluster stellar population. We confirm the presence of multiple stellar populations in NGC 1783. Our photometry strongly suggests that the MSTO of this cluster is formed by two distinct branches. In seven clusters (ESO057-SC075, HODGE7, NGC 1852, NGC 1917, NGC 1987, NGC 2108, and NGC 2154) we observed an intrinsic broadening of the MSTO that may suggest that these clusters have experienced a prolonged period of star formation that span a period between 150 and 250 Myr. The CMDs of IC 2146, NGC 1644, NGC 1652, NGC 1795 and NGC 1978 show no evidence of spread or bimodality within our photometric precision. In summary 70±25% of our sample are not consistent with the simple, single stellar population hypotesis.

1. Introduction

Nearly all the clusters that have been resolved into individual stars exhibit a color-magnitude diagram (CMD) consistent with the stars belonging to a single, simple stellar population. In recent years, however, thanks to the improving precision of instruments and techniques (mainly from space), the discovery of multiple populations of stars in stellar clusters is challenging this traditional picture and has led to new views on how clusters form and evolve.

Thus far, photometry has revealed multiple stellar populations in a few Galactic Globular Clusters (GGCs) i. e. Omega Centauri (Anderson 1997, Bedin et al. 2004, Piotto et al. 2005, Sollima et al. 2007, Villanova et al. 2007), NGC 2808 (D'Antona et al. 2005, Piotto et al. 2007), NGC 1851 (Milone et al. 2008), and NGC 6388 (Piotto 2008), also in some intermediate-age Large Magellanic Cloud (LMC) clusters (Bertelli et al. 2003, Mackey & Broby Nielsen 2007 [M07], Mackey et al. 2008 [M08]) and in the Small Magellanic Cloud (SMC) cluster NGC 419 (Glatt et al 2008a). Each of the above clusters exhibits a different pattern of age spread and/or chemical enrichment. It is clear that the star-formation history differs from cluster to cluster (see Piotto 2008 for a review).

Send offprint requests to: A. P. Milone

⋆ Based on observations with the NASA/ESA *Hubble Space Telescope*, obtained at the Space Telescope Science Institute, which is operated by AURA, Inc., under NASA contract NAS 5-26555.

There is additional photometric evidence that other clusters exhibit some kind of population multiplicity. Marino et al. (2008) found photometric evidence of two distinct stellar populations among the red giant branch (RGB) stars of M4. Yong et al. (2008) find abundance variations in NGC 6752 that correlate with the Strömgren *cy* index, and show eight other clusters that present a similar *cy* spread in their giant branches.

In addition, many GGCs, including those with no photometric evidence for multiple populations, exhibit large star-to-star variations in their chemical abundances (see Gratton et al. 2004 for a review). Almost all GGCs have homogeneous Fe-peak-element abundances (with the only exception being Omega Centauri, hereafter ω Cen), but they show a significant dispersion in CNO, Na, Mg, Al and *s*-process elements. The pattern of chemical abundances in GGCs must be primordial as it is observed not only among RGB or asimptotic giant branch (AGB) stars, but also among the sub giant branch (SGB), and most importantly among unevolved stars on the MS (Gratton et al. 2001, 2004). The presence of a well defined pattern among Na, O, Mg, and Al suggests that most of the GGCs may have hosted multiple episodes of star formation separated by few hundred Myrs (D'Antona & Caloi, 2008).

Unfortunately, in an old population, such a difference in age corresponds to a difference of few hundredths of a magnitude at the level of the MS turn-off (TO) and SGB. At the moment it is not possible to firmly establish the presence of a spread in a cluster's MSTO with this amplitude given the presence of differential reddening and difficulties in doing systematically accurate crowded-field photometry at this level of precision.

The families of young and intermediate-age massive clusters that populate the Large and the Small Magellanic Cloud offer us precious opportunities to photometrically search for multiple stellar populations because, in the CMD of a 1-3 Gyr old cluster, an age interval of 200-300 Myr corresponds to a magnitude difference of a few tenths of a magnitude. Two populations with such a difference could easily be distinguished even at the distance of the Magellanic Clouds (MC).

Indeed, recent photometric studies of LMC clusters have demonstrated that the presence of multiple stellar populations is not a peculiarity of the most massive Galactic GGCs. Bertelli et al. (2003) have compared a CMD of NGC 2173 from FORS/VLT data with Padova models and suggested for this LMC cluster a prolonged star-formation episode spanning a period of about 300Myr. In a recent paper, M08 found that the main-sequence turn off (MSTO) for NGC 1783 reveals a much larger spread in color than can be explained by photometric errors. M07 and M08 also revealed the presence of a double MSTO in the rich intermediate-age clusters NGC 1846 and NGC 1806 of the LMC, and suggested that their CMDs unveil the presence of two populations with an age difference of $\sim$ 300 Myr.

Driven by these results on Galactic and LMC clusters, we have undertaken an analysis of archival *HST* images of LMC and SMC clusters with the purpose of measuring the frequency of clusters with evidence of multiple or prolonged star formation. The clusters that have been analysed cover a wide range of ages, from $\sim 10^6$ to $\sim 10^{10}$ yr. Since the search of multiple populations is carried out through analysis of CMDs, the study of clusters with different ages requires different analysis.

In this paper, which is the first of a series, we show our entire sample of ACS/WFC CMDs for forty-seven LMC and SMC stellar clusters and present a detailed study of sixteen intermediate-age LMC clusters (between $\sim$ 1and $\sim$ 3Gyr). The paper is organized as follow. Section 2 describes the data and the data reduction techniques. In Section 3 we present the CMDs of the sixteen intermediate-age clusters. In Section 4, we confirm the split of the MSTO of NGC 1806 and NGC 1846, and observe, for the first time, two distinct MSTOs in NGC 1751. We analyse in details the CMD of these clusters and measure the fraction of stars belonging to each of their MSTO populations. We confirm the presence of multiple stellar populations in NGC 1783 and suggest that the MSTO of this cluster should be formed by two distinct branches. In Section 5 we note an anomalous spread around the MSTO of seven clusters: ESO057-SC075, HODGE 7, NGC 1852, NGC 1917, NGC 1987, NGC 2108, and NGC 2154. In Section 6 we demonstrate that the observed spread in the MSTO region of these clusters must be real, as it cannot be due to differential reddening, field contamination, photometric errors or binary stars. In Section 7 we determine the cluster ages and the age differences among different stellar populations in the same cluster through isochrone fitting. Finally, Section 8 includes a short summary of our results.

2. Observation and data reduction

In order to investigate the presence of multiple stellar populations in Magellanic Cloud clusters we searched the MAST STScI-archive for *HST* images collected with the Wide Field Channel (WFC) of the Advanced Camera for Surveys (hereafter ACS/WFC). We found useful images for 53 clusters from GO 9891 (PI: G. F. Gilmore), GO 10395 (PI: J. S. Gallagher) and GO 10595 (PI: P. Goudfrooij). The result of this search is presented in Tab. 1 for 47 clusters from GO 9891 and GO 10595, while the GO 10396 data-set described in Table 1 of Glatt et al. (2008b) (which includes six SMC clusters) will be used in a future paper focused on SMC.

The photometric reduction of the ACS/WFC data has been carried out using the software presented and described in detail in Anderson et al. (2008). It consists in a package that analyses all the exposures of each cluster simultaneously in order to generate a single list of stars for each field. Stars are measured independently in each image by using the best available PSF models from Anderson & King (2006).

This routine was designed to work well in both crowded and uncrowded fields and it is able to detect almost every star that can be detected by eye. It takes advantage of the many independent dithered pointings of each scene and the knowledge of the PSF to avoid including artifacts in the list. Calibration of ACS photometry into the Vega-mag system has been performed following recipes in Bedin et al. (2005) and using the zero points given in Sirianni et al. (2005).

ID	DATE	EXPOSURES	FILT	PROGRAM	ID	DATE	EXPOSURES	FILT	PROGRAM
ESO 057-SC075	Nov 05 2006	55s+2×340s	F435W	10595	NGC 1806	Aug 08 2003	300s	F555W	9891
	Nov 05 2006	25s+2×340s	F555W	10595		Aug 08 2003	200s	F814W	9891
	Nov 05 2006	15s+2×340s	F814W	10595		Sep 29 2005	90s+2×340s	F435W	10595
ESO 121-SC03	Oct 07 2003	330s	F555W	9891		Sep 29 2005	40s+2×340s	F555W	10595
	Oct 07 2003	200s	F814W	9891		Sep 29 2005	8s+2×340s	F814W	10595
HODGE 7	Oct 07 2003	330s	F555W	9891	NGC 1846	Oct 08 2003	300s	F555W	9891
	Oct 07 2003	200s	F814W	9891		Oct 08 2003	200s	F814W	9891
IC 1660	Aug 13 2003	73s	F555W	9891		Jan 01 2006	90s+2×340s	F435W	10595
	Aug 13 2003	58s	F814W	9891		Jan 01 2006	40s+2×340s	F555W	10595
IC 2146	Jul 07 2003	250s	F555W	9891		Jan 01 2006	8s+2×340s	F814W	10595
	Jul 07 2003	170s	F814W	9891	NGC 1852	Oct 07 2003	330s	F555W	9891
KRON 1	Aug 27 2003	480s	F555W	9891		Oct 07 2003	200s	F814W	9891
	Aug 27 2003	290s	F814W	9891	NGC 1854	Oct 07 2003	50s	F555W	9891
KRON 21	Aug 22 2003	480s	F555W	9891		Oct 07 2003	40s	F814W	9891
	Aug 22 2003	290s	F814W	9891	NGC 1858	Oct 08 2003	20s	F555W	9891
KRON 34	Aug 12 2003	165s	F555W	9891		Oct 08 2003	20s	F814W	9891
	Aug 12 2003	130s	F814W	9891	NGC 1872	Sep 21 2003	115s	F555W	9891
LYNDSAY 1	Jul 11 2003	480s	F555W	9891		Sep 21 2003	90s	F814W	9891
	Jul 11 2003	290s	F814W	9891	NGC 1903	Jui 02 2004	50s	F555W	9891
LYNDSAY 38	Jun 03 2004	480s	F555W	9891		Jui 02 2004	40s	F814W	9891
	Jun 03 2004	290s	F814W	9891	NGC 1917	Oct 07 2003	300s	F555W	9891
LYNDSAY 91	Aug 24 2003	435s	F555W	9891		Oct 07 2003	200s	F814W	9891
	Aug 24 2003	290s	F814W	9891	NGC 1928	Aug 23 2003	330s	F555W	9891
LYNDSAY 113	Jun 03 2004	480s	F555W	9891		Aug 23 2003	200s	F814W	9891
	Jun 03 2004	290s	F814W	9891	NGC 1939	Jul 27 2003	330s	F555W	9891
LYNDSAY 114	Aug 07 2003	480s	F555W	9891		Jul 27 2003	200s	F814W	9891
	Aug 07 2003	290s	F814W	9891	NGC 1943	Oct 07 2003	50s	F555W	9891
NGC 265	Aug 24 2003	29s	F555W	9891		Oct 07 2003	40s	F814W	9891
	Aug 24 2003	29s	F814W	9891	NGC 1953	Oct 07 2003	115s	F555W	9891
NGC 294	Aug 24 2003	165s	F555W	9891		Oct 07 2003	90s	F814W	9891
	Aug 24 2003	130s	F814W	9891	NGC 1978	Oct 07 2003	300s	F555W	9891
NGC 422	Oct 07 2003	73s	F555W	9891		Oct 07 2003	200s	F814W	9891
	Oct 07 2003	58s	F814W	9891	NGC 1983	Oct 07 2003	20s	F555W	9891
NGC 602	Aug 16 2003	29s	F555W	9891		Oct 07 2003	20s	F814W	9891
	Aug 16 2003	29s	F814W	9891	NGC 1987	Oct 07 2003	250s	F555W	9891
NGC 1644	Oct 07 2003	250s	F555W	9891		Oct 07 2003	170s	F814W	9891
	Oct 07 2003	170s	F814W	9891		Oct 18 2006	90s+2×340s	F435W	10595
NGC 1652	Oct 07 2003	300s	F555W	9891		Oct 18 2006	40s+2×340s	F555W	10595
	Oct 07 2003	200s	F814W	9891		Oct 18 2006	8s+2×340s	F814W	10595
NGC 1751	Oct 07 2003	300s	F555W	9891	NGC 2002	Aug 23 2003	20s	F555W	9891
	Oct 07 2003	200s	F814W	9891		Aug 23 2003	20s	F814W	9891
	Oct 17-18 2006	90s+2×340s	F435W	10595	NGC 2010	Oct 07 2003	20s	F555W	9891
	Oct 17-18 2006	40s+2×340s	F555W	10595		Oct 07 2003	20s	F814W	9891
	Oct 17-18 2006	8s+2×340s	F814W	10595	NGC 2056	Aug 08 2003	170s	F555W	9891
NGC 1755	Aug 23 2003	50s	F555W	9891		Aug 08 2003	120s	F814W	9891
	Aug 23 2003	40s	F814W	9891	NGC 2107	Oct 07 2003	170s	F555W	9891
NGC 1756	Aug 12 2003	170s	F555W	9891		Oct 07 2003	120s	F814W	9891
	Aug 12 2003	120s	F814W	9891	NGC 2108	Aug 16 2003	250s	F555W	9891
NGC 1783	Oct 07 2003	250s	F555W	9891		Aug 16 2003	170s	F814W	9891
	Oct 07 2003	170s	F814W	9891		Aug 22 2006	90s+2×340s	F435W	10595
	Jan 01 2006	90s+2×340s	F435W	10595		Aug 22 2006	40s+2×340s	F555W	10595
	Jan 01 2006	40s+2×340s	F555W	10595		Aug 22 2006	8s+2×340s	F814W	10595
	Jan 01 2006	8s+2×340s	F814W	10595	NGC 2154	Oct 08 2003	300s	F555W	9891
NGC 1795	Aug 09 2003	300s	F555W	9891		Oct 08 2003	200s	F814W	9891
	Aug 09 2003	200s	F814W	9891	RETICULUM	Sep 21 2003	330s	F555W	9891
NGC 1801	Oct 08 2003	115s	F555W	9891		Sep 21 2003	200s	F814W	9891
	Oct 08 2003	90s	F814W	9891					

Table 1. Description of the data sets.

2.1. Selection of a sample of best measured stars

Stars can be poorly measured for several reasons: crowding by nearby neighbours, contamination by cosmic-rays (CRs) or image artifacts such as hot pixels or diffraction spikes. The goal of the present work is to clearly identify multi-populations. For this purpose we need to select the best-measured stars in the field (i.e., those with the lowest random and systematic errors), but we also need to have a large enough statistical sample to be able to identify secondary sequences that may have many fewer members than the primary ones.

The software presented by Anderson et al. (2008) provides very valuable tools to reach this goal. In addition to the stellar fluxes and positions it provides a number of parameters that can be used as diagnostics of the reliability of photometric measurements. Specifically these are:

- the rms of the magnitudes measured in different exposures ($rms_{m_{\rm F435W}}$, $rms_{m_{\rm F555W}}$, and $rms_{m_{\rm F814W}}$, available only for clusters with more than one exposure in the same filter, cfr. Tab. 1);
- the rms of the positions measured in different exposures transformed in a common distortion-free reference frames ($rms_{\rm X}$, and $rms_{\rm Y}$);
- the residuals to the PSF fit for each star ($q_{m_{\rm F435W}}$, $q_{m_{\rm F555W}}$, and $q_{m_{\rm F814W}}$; this is what Anderson et al. 2008, define as *quality fit*);
- the ratio between the estimated flux of the star in a 0.5 arcsec aperture, and the flux from neighboring stars within

the same aperture ($o_{m_{\rm F435W}}$, $o_{m_{\rm F555W}}$, and $o_{m_{\rm F814W}}$, again see Anderson et al. 2008 for details).

We used these parameters to select a sub-sample of stars with the best photometry.

In the five left panels of Fig. 1, we show the criteria that we have used to select the sample of stars with the best photometry in the F435W band for NGC 1806. The photometric system at this stage is kept in instrumental magnitudes, $-2.5\log_{10}$(flux), where the flux is expressed in photo-electrons recorded in the reference exposure.

We note a clear trend of the quality-fit and *rms* parameters as a function of the magnitude due to the decreasing signal-to-noise ratio (S/N). In order to select well-measured stars at different S/N we adopted the following procedure.

We began by dividing all the stars into magnitude bins. The size of each bin varied from one cluster to another depending on the number of stars; for each of them, we computed the median *rms* (q) and the 68.27$^{\rm th}$ percentile (hereafter σ). The median was derived recursively: after each computation, all stars exceeding four times σ were provisionally rejected until the next iteration and the median was recomputed. This procedure was repeated until two subsequent measures of the median differ by less than the 1% of the value.

Finally, we arrived at the red line of Fig. 1 by adding to the median of each bin N times σ. This gave us the red circles, which we then fitted with a spline. All stars below the red line in each plot have been flagged as well-measured. The factor N ranges from 5 to 6, and has been chosen in order to draw the boundaries that follow the bulk of the distribution of each parameter value.

The neighbour-contamination parameters do not show a clear trend with magnitude, so we simply flagged as well-measured all the stars with $o_{m_{\rm F435W,\ F555W,\ F814W}} < 5$.

Obviously, the *rms* of the magnitudes was not available in the case of clusters with only one image per band (HODGE 7, IC 2146, NGC 1644, NGC 1652, NGC 1795, NGC 1852, NGC 1917, NGC 1978, and NGC 2154). In such cases those selections were not applied.

In the right panels of Fig. 1 we show the CMD of all the measured stars of NGC 1806 (top) and of stars that pass all the selection criteria (bottom).

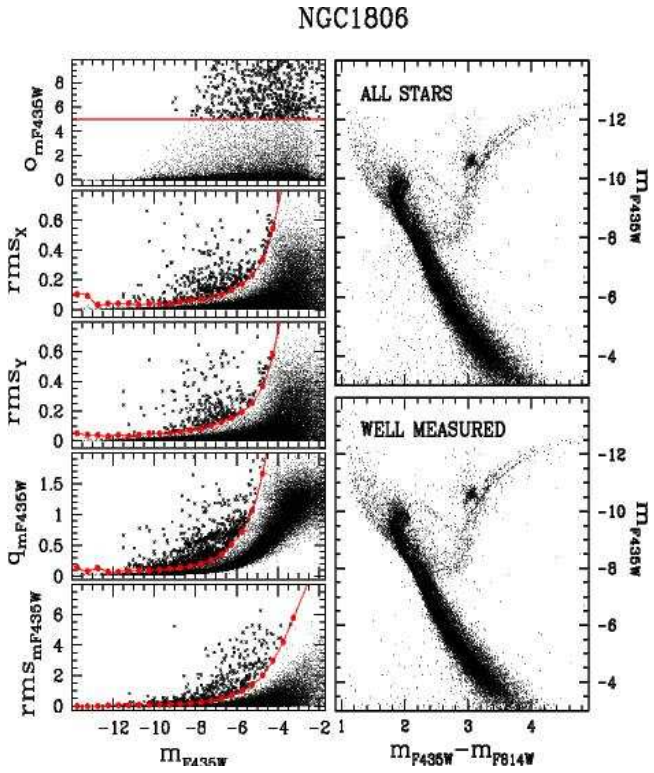

Fig. 1. Diagnostic parameters used to select the stars with the best photometry are plotted as a function of $m_{\rm F435W}$ for NGC 1806. Red lines separate the well-measured stars (thin points) from those that are more likely to have a poorer photometry (thick points). On the right we compare the CMD of all the measured stars (top) and of stars that pass our criteria of selection (bottom).

2.2. Artificial-star tests

The artificial-star (AS) experiments used in this paper have been run following the procedures described in Anderson et al. (2008).

First of all, for each cluster, we produced an input list with about 10^5 stars located on the entire ACS field of view. It includes the coordinates of the stars ($X_{\rm in}$, $Y_{\rm in}$) in the reference frame, and the magnitudes in the F435W (or F555W) and F814W bands ($mv_{\rm in}$, $mi_{\rm in}$). We generated the artificial stars with a flat luminosity function in the F814W band and with instrumental magnitudes from -5 to -14. We placed artificial stars fainter than the MSTO on the MS ridge line that is determined as described in section 6.2.1 and added artificial stars brighter than the MSTO along the isochrone that best fits the observed CMD (see section 7).

The program described in Anderson et al. (2008) allows artificial-star tests to be performed for one star at a time and entirely in software guaranting that artificial stars will never interfere with each other, no matter how many tests are done. Therefore it makes very simple to do artificial star tests because it is not necessary to add an array of non-interfering stars on the images, reducing all the images each time. For each star in the input list, the routine adds the star to each exposure at the appropriate place with the appropriate flux, and measures the images in the same manner as real stars, producing the same output parameters as in section 2.1. If the input and the output positions differ by less than 0.5 pixel and the fluxes differ by less than 0.75 magnitudes, than the artificial star is considered as found.

Artificial stars played a crucial role in this analysis; they allowed us to determine the completeness level of our sample and to measure the fraction of chance-superposition "binaries". The completeness depends on the crowding conditions as well as on stellar luminosity. Our procedures account for both of these. Our goal in the AS tests is to probe how incompleteness and photometric errors vary with crowding or brightness. So, we generated a list of artificial stars that had colors that placed

them on the average cluster sequence and positions drawn from the overall cluster radial distribution.

We divided the ACS/WFC field for each cluster into 5 concentric annuli centered on the cluster center, and within each annulus we examined the AS results in eight magnitude bins, from −14 to −5. For each of these 5×8 grid points, we then determined the average completeness by taking the ratio of the recovered to input artificial stars within that bin. This grid then allowed us to estimate the completeness for any star at any position within the cluster. As an example, the left panel of Fig. 2 shows the completeness as a function of the instrumental $m_{\rm F814W}$ magnitude in each of the five annuli we used to divide the field of NGC 1806. Finally, we interpolated the grid points and derived the completeness value associated with each star. The right panel of Fig. 2 shows the completeness contours in the radius versus $m_{\rm F814W}$ magnitude plane. Continuous lines correspond to completeness levels of 0.25, 0.50 and 0.75. Dotted lines indicate differences of completeness of 0.05.

3. The cluster CMDs

In Fig. 3 we show the instrumental $m_{\rm F555W}$ versus $m_{\rm F555W} - m_{\rm F814W}$ CMDs of all the 47 clusters from GO 9891 and GO 10595 presented in Section 2. It is clear from this figure that our sample contains clusters at many different stages of evolution. This paper will deal with the CMDs of the sixteen intermediate-age clusters (from ∼ 1 to ∼ 3 Gyr). The other clusters will be covered in forthcoming papers. All selected intermediate age clusters are LMC members.

Most of the CMDs plotted in Fig. 3 show considerable evidence of contamination, mainly due to MC field stars. For the purposes of this paper, it is crucial to determine as well as possible the stellar distribution in the field-star CMD, since without such attention, field sequences could be erroneously attributed to the cluster and interpreted as an additional population.

Since most of the clusters of our sample cover a small portion of the ACS/WFC field of view, we can easily isolate a CMD that is representative of the field population surrounding the cluster by selecting the portion of the ACS/WFC image that are most distant from the cluster center, so that the contamination of cluster members should be negligible and, in many cases, almost absent.

In order to minimize the fraction of field stars in the cluster CMD, we selected two regions with the same area. The first region, which below we will call the 'cluster field', is centered on the cluster and includes the region with the highest density of cluster members (with the only exception of NGC 1978, where we chose an annulus around the cluster center in order to exclude the crowded cluster core). The second region is far enough from the cluster center that very few cluster stars would be expected to be present there. We will call this field 'reference field' and its stars should be representative of the typical population in front of and behind the cluster. Since cluster stars in the vicinity of the MSTO are the main target of the present study, we defined the area of these regions such that the density of stars within a magnitude from the TO, namely with $m_{\rm F814W} < (m^{\rm TO}_{\rm F814W} + 1)$, in the cluster field would be at least a fixed number (N) of times that of the reference field. In most cases we could set $N = 5$, which would mean that even without field correction, we have at most a 20% contamination. An exception is NGC 1917 which is projected upon a densely populated region of the LMC. In this case we used $N = 3$. For the most populated clusters (IC 2146, NGC 1806, NGC 1846, and NGC 1978) we adopted $N = 10$.

In Fig. 4, we compare the CMDs of the cluster and reference fields for the sixteen intermediate age clusters that have been studied in this paper. All the reference-field CMDs selected with this criterion share a broadened, young main sequence and a 5-6 Gyr old stellar population that departs from the MS at around $m_{\rm F555W} = 22.5$ and populate the evolved portions of the CMD. In Sec. 6.1 we will use the CMDs of the reference field to decontaminate the CMD of the cluster.

3.1. Differential reddening

It is well known that differential reddening causes a shift of all the CMD features parallel to the reddening line and tends to randomly broaden them. A quick look at the CMDs presented in this paper shows that most of the RGBs and AGBs are narrow and well defined, and that the HB red-clump is compact. Moreover, we have divided the cluster field into many subregions (the exact number varies from one cluster to another, depending on the number of stars) and compared the CMDs of stars located in each of them. In most cases, we found no evidence for an offset among the CMDs and therefore, any variations of reddening should be negligible.

Two exceptions to this reddening-free rule are NGC 1751 and NGC 2108. We show their CMD in Fig. 5 and 6. The confused shape of the HB red-clumps and of other primary features suggests the presence of differential reddening. Since differential reddening acts along the direction of the reddening arrow shown at the lower left, sequences (such as the SGB) that are aligned perpendicular to the reddening line are most affected.

For this reason, a search for a possible split or a spread around the MSTO requires an accurate correction of the effects produced by differential reddening on the observed CMD. In order to correct for differential reddening, we have used the procedure described in Sarajedini et al. (2007). Briefly: we define the fiducial main sequence for the cluster and tabulate, at a grid of points across the field, how the observed stars in the vicinity of each grid point may systematically lie to the red or the blue of the fiducial sequence; this systematic color offset is indicative of the local differential reddening.

In the lower panel of Fig. 5, we show the corrected CMD of NGC 1751. It should be noted how, after the correction has been applied, all the main features of the CMD become narrower and clearly defined, confirming that most of the effects of differential reddening have been removed. The improvement of the CMD is particularly evident for the stars of the HB red-clump; the tightness along the reddening line of this clump means that the spread (or split) we see in the MSTO cannot be due to differential reddening. Figure 6 illustrates the effects of the reddening correction in NGC 2108. The total amount of differential reddening within the clus-

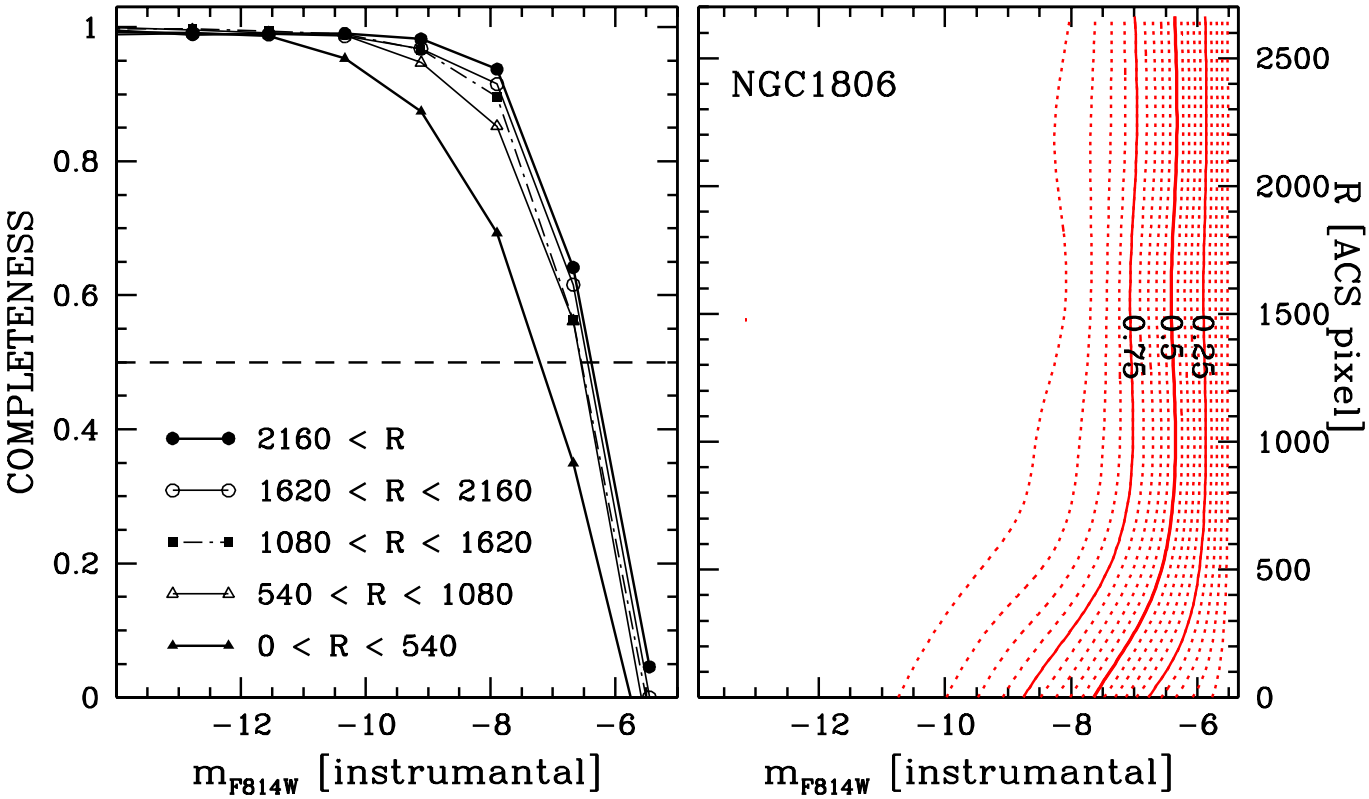

Fig. 2. Left: Completeness as a function of the m_{F814W} magnitude in five annuli. Right: Completeness contours in the radial distance versus m_{F814W} magnitude plane.

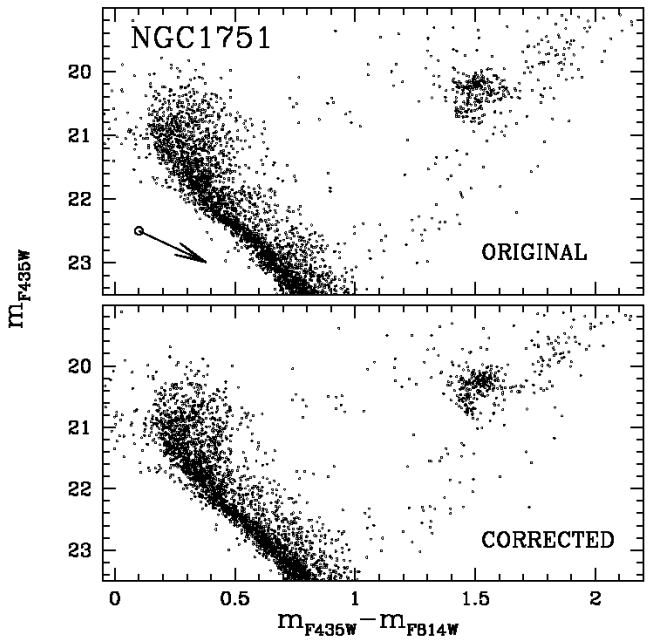

Fig. 5. Comparison between the CMD of NGC 1751 before (top panel) and after (bottom panel) the correction for differential reddening. The arrow indicates the reddening direction.

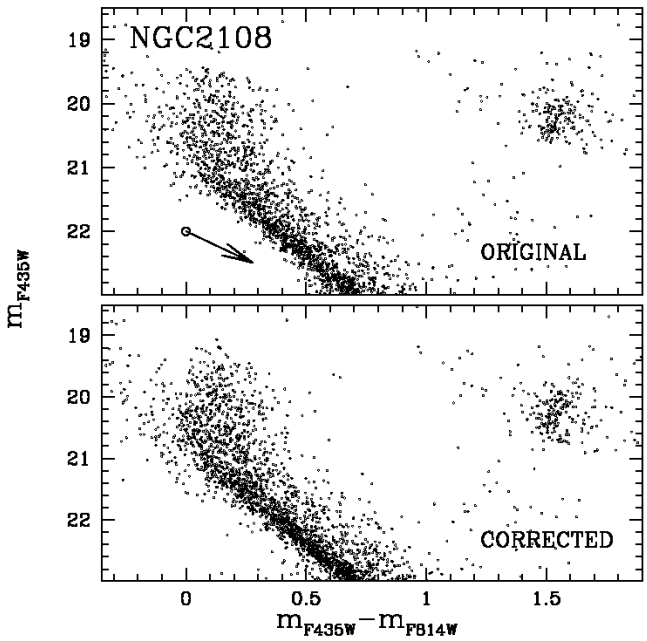

Fig. 6. As in Fig. 5 for NGC 2108.

ter region is Δ *E(F435W-F814W)*=0.10 for NGC 1751 and Δ *E(F435W-F814W)*=0.08 for NGC 2108.

The two clusters that suffer of a sizable differential reddening are not at any particular angular distance from the center of the LMC, or with respect to the Milky Way, compared to the other forteen clusters. They might just fall in some gas-dust

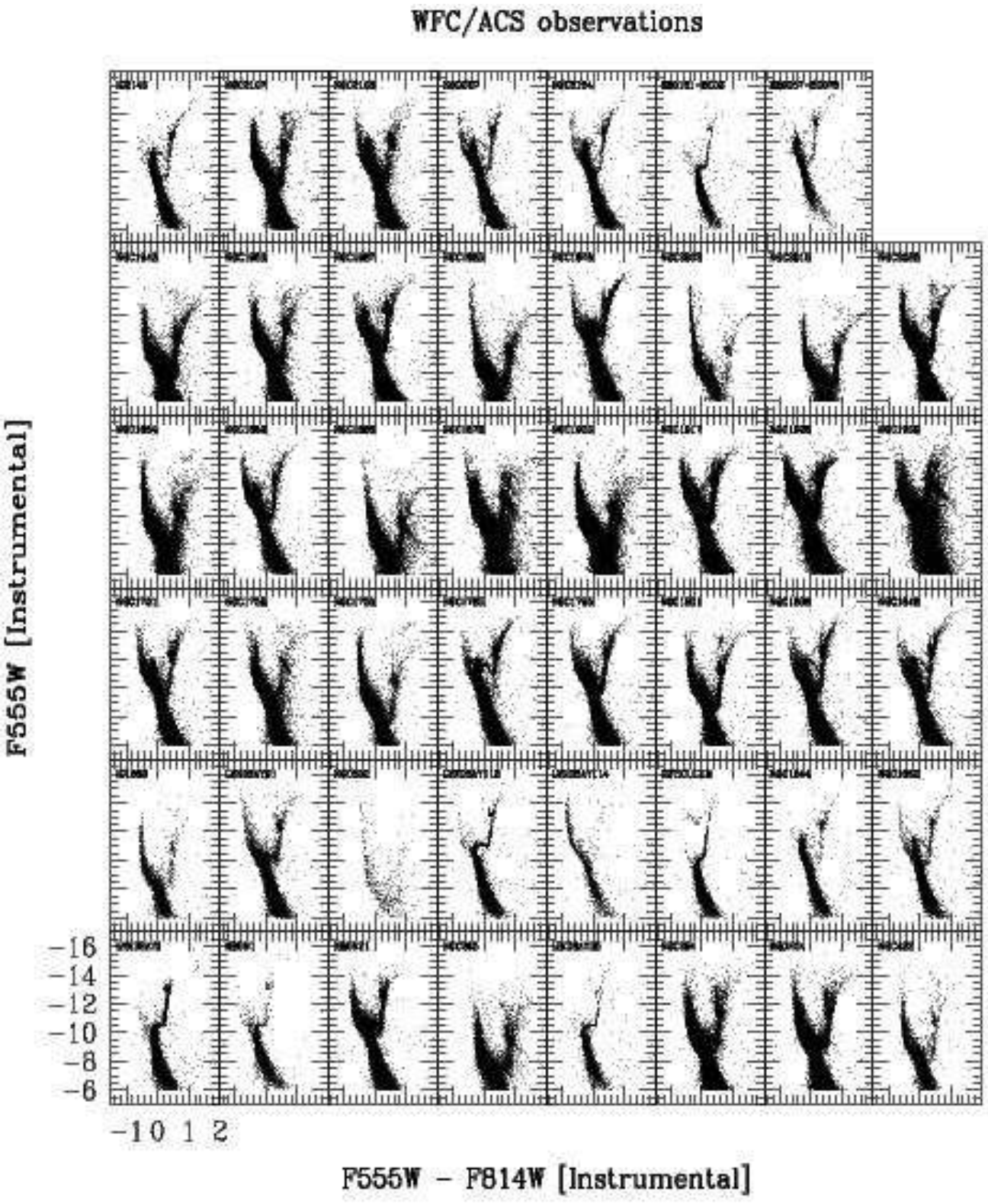

Fig. 3. Instrumental m_{F555W} vs. $m_{F555W} - m_{F814W}$ for 47 MCs clusters.

complex structure poorly known, and/or with a limited spatial extension.

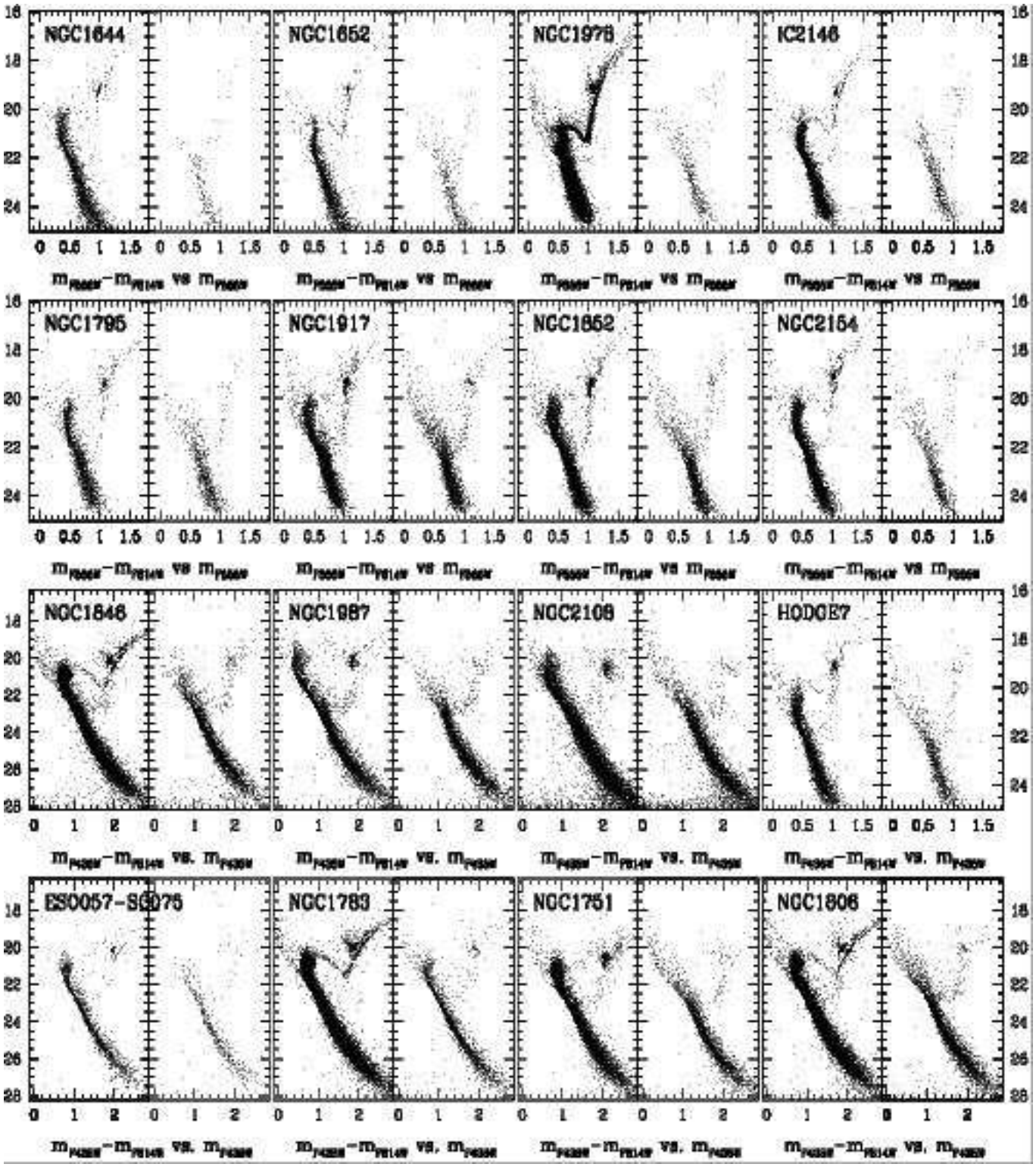

Fig. 4. Comparison of the CMD of cluster and reference fields for the 16 selected intermediate-age clusters.

4. Clusters with a double MSTO: NGC 1806, NGC 1846 and NGC 1751

At least three clusters of our sample clearly show two distinct MSTOs: NGC 1846, NGC 1806, and NGC 1751. The split is evident in the CMDs of the cluster fields that are shown in Fig. 7, 8 and 9, and is exalted by the Hess diagram in the inset. The presence of two, distinct TOs in NGC 1806 and NGC 1846 was discovered by M07 and M08, who also found no difference in the spatial distribution between the stars in the brighter and fainter MSTOs (hereafter bMSTO and fMSTO). In this work, we take advantage from the high photometric quality of our CMDs to measure the fraction of stars belonging to each turnoff

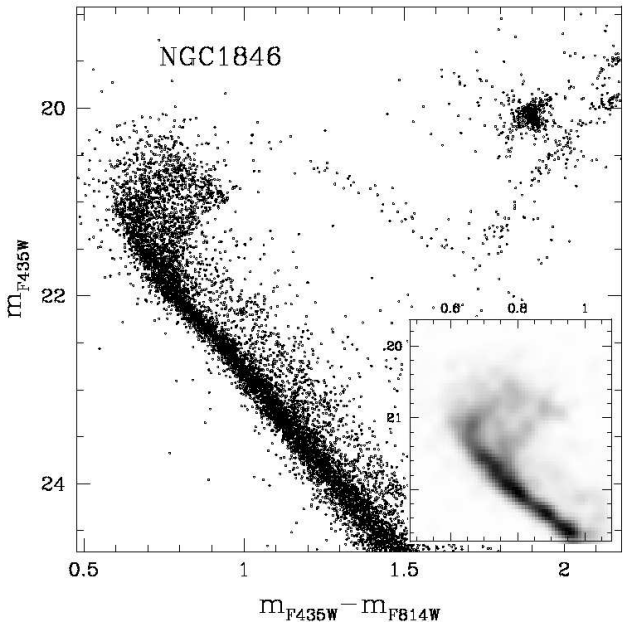

Fig. 7. CMD of NGC 1846. All detected sources in the inner field that successfully passed all the selection criteria have been plotted. In the inset we show the Hess diagram for the CMD region around the MSTO.

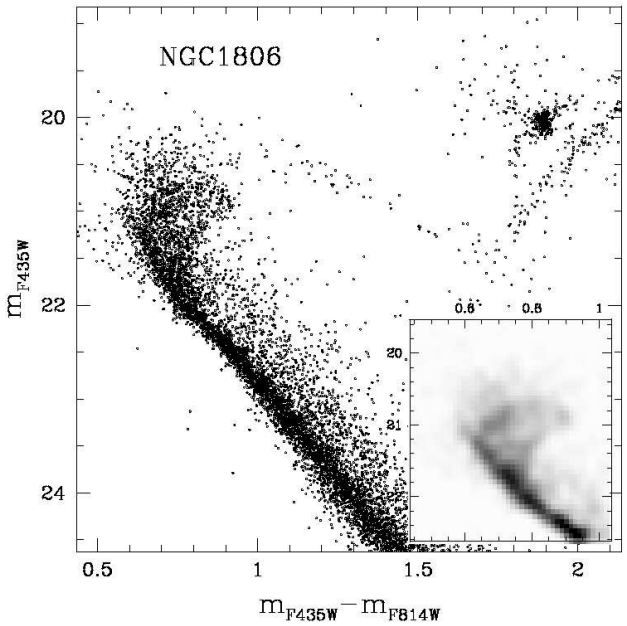

Fig. 8. As in Fig. 7 for NGC 1806.

population. To do this, it is necessary to select and compare the two groups of bMSTO and fMSTO.

This procedure is illustrated in Fig. 10 for NGC 1806. We used the CMD of the cluster field, with foreground/background contamination removed as described in Section 6.1. We began by finding the isochrones that went through the two sequences and the giant branch (as it will be described in details in section 7). These are the red and the blue lines. We then defined by hand two pairs of reference points: $P_{1,f}$ and $P_{2,f}$ on the fMSTO isochrone and $P_{1,b}$ and $P_{2,b}$ on the bMSTO isochrone. The two pairs of points have been chosen with the criterion of delimiting the region of the CMD where the split is more evident and have been used to draw the grey lines in panel (a). Only stars contained in the region between these lines have been used for the following analysis.

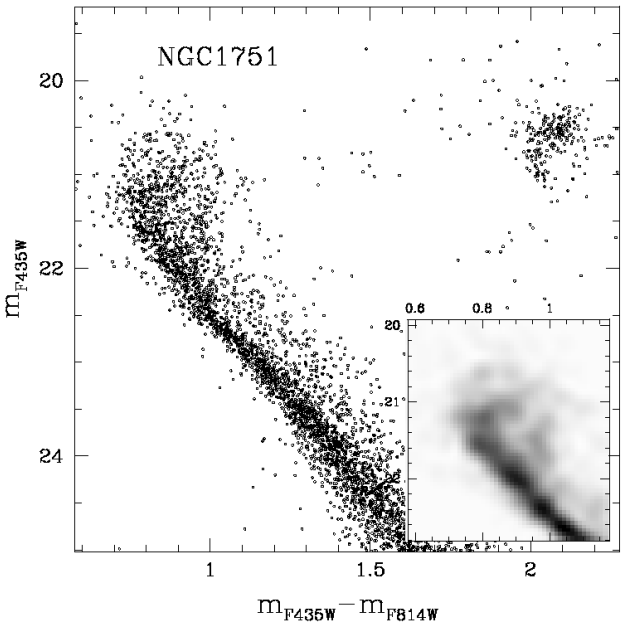

Fig. 9. As in Fig. 7 for NGC 1751.

In panel (b), we have shifted and rotated the reference frame such that the new origin corresponds to $P_{1,f}$ and the abscissa goes from $P_{1,b}$ to $P_{1,f}$. For simplicity, in the following, we will refer to the abscissa and ordinate of this reference frame as 'color' and 'magnitude'. The red dashed line is a fiducial line through the region close to the fMSTO. We drew it by marking on the region close to the fMSTO four points, equally spaced in 'magnitude' and drawing, a line through them by means of a spline fit.

In panel (c) the 'color' of this line has been subtracted from the color of each star, and the 'magnitude' of each star has been divided by the 'magnitude' of a stars with the same 'color' that lie on the line that goes from $P_{1,f}$ to $P_{1,b}$.

For the analysis that follows, we have divided the Δ'magnitude' range into N bins. We used $N = 4$ for NGC 1806 and NGC 1846 and $N = 2$ for the less populated NGC 1751. In each of them, we have determined the fraction of stars belonging to each MSTO as follows. Our aim was to model the Δ'color' distribution by fitting the sum of two partially overlapping gaussians, but we need to reduce the influence of outliers (such as stars with poor photometry, residual field stars and binaries). To this end, we did a preliminary fit of the gaussians using all available stars, then we rejected all the stars distant more than two σ_b from the bMSTO and less than 2 σ_f from the fMSTO and repeated the fit (where the σ's are those of the

best fitting gaussians in each Δ'magnitude' bin fitted to the fMSTO and bMSTO respectively).

The continuous vertical lines show the centers of the best-fitting gaussians in each Δ'magnitude' interval. The red dashed line is located two σ_f on the "blue" side of the fMSTO and the blue line runs two σ_b on the "red" side of the bMSTO,

It is important to notice here that, to each point ($P_{1,f(b)}$, $P_{2,f(b)}$) that we have arbitrarely selected on the two isochrones with the only purpose of disentangle the two SGBs, corresponds a mass ($\mathcal{M}_{P1f(b)}$, $\mathcal{M}_{P2f(b)}$). In order to obtain a more correct measure of the fraction of stars in each of the two population (f_{bMSTO}, f_{fMSTO}) it must be noted that we are dealing with two different mass intervals ($\mathcal{M}_{P2f} - \mathcal{M}_{P1f} \neq \mathcal{M}_{P2b} - \mathcal{M}_{P1b}$) and we have to compensate for two facts: first, more massive stars are more rare, and second, more massive stars evolve faster.

We calculated the fraction of stars in each branch as:

$$f_{bMSTO} = \frac{\frac{A_b}{N_b/N_f}}{A_f+\frac{A_b}{N_b/N_f}}$$
$$f_{fMSTO} = \frac{A_f}{A_f+\frac{A_b}{N_b/N_f}}$$

where A_b and A_f are the area of the gaussians that best fit the bMSTO and the fMSTO, and $N_{f(b)} = \int_{P_{1,f(b)}}^{P_{2,F(b)}} \phi(\mathcal{M})d\mathcal{M}$, being adopting for $\phi(\mathcal{M})$ the Salpeter (1955) IMF.

We find that 74±4 % of stars of NGC 1806 belong to the bMSTO and 26±4% to the fMSTO. In the case of NGC 1846 we have 75±3 % of stars in the bMSTO and 25±3 % in the fMSTO. Finally, 69±4 % of the NGC 1751 stars belong to the bMSTO and the 31±4 % to the fMSTO. Interestingly enough, a similar population ratio between the bright and the faint SGB ratios has been found in the Galactic globular clusters NGC 1851 (Milone et al. 2008) and NGC 6388 (Piotto et al, in preparation). We note here that D'Antona and Coloi (2008) predict that more than 50% of the cluster stars must be coming from the second (younger) population in their intermediate mass AGB ejecta pollution scenario proposed to explain multiple populations in star clusters.

4.1. The (double ?) MSTO of NGC 1783.

A spread in color around the MSTO of NGC 1783 was first noted by Mucciarelli et al. (2007). Unfortunately their $m_{\rm F555W}$ versus $m_{\rm F555W} - m_{\rm F814W}$ CMD had low photometric accuracy, because it was obtained from the GO 9891 images alone. Therefore, they were unable to distinguish between the intrinsic spread in color and the broadening expected by photometric uncertainties. M08 obtained a CMD for this cluster from data with higher S/N (using both GO 10595 and GO 9891 images) and demonstrated that NGC 1783 shows a much larger spread in color than what would be expected by photometric errors alone.

Our CMD of NGC 1783 is shown in Fig. 11 and clearly confirms the anomalous spread around the MSTO. In addition, the Hess diagram in the inset reveals a splitted MSTO and strongly suggests that the apparent spread could be attributed to the presence of two distinct branches which are closely spaced and poorly resolved by the observations.

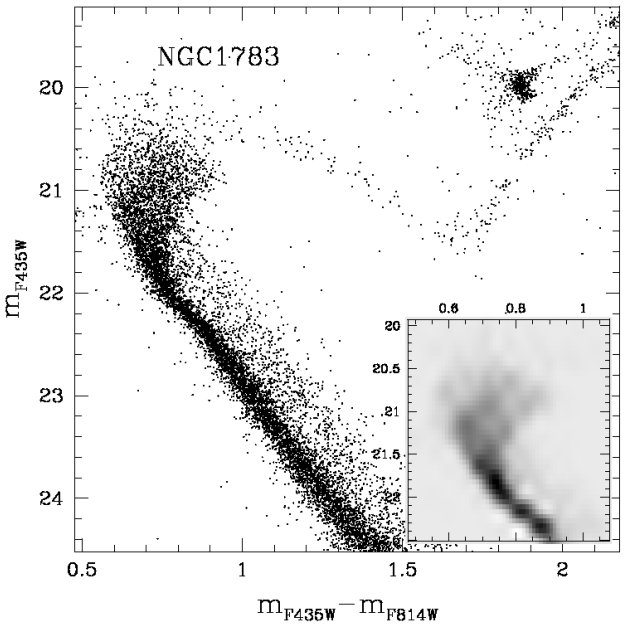

Fig. 11. As in Fig. 7 for NGC 1783.

5. Possible evidence of prolonged star formation

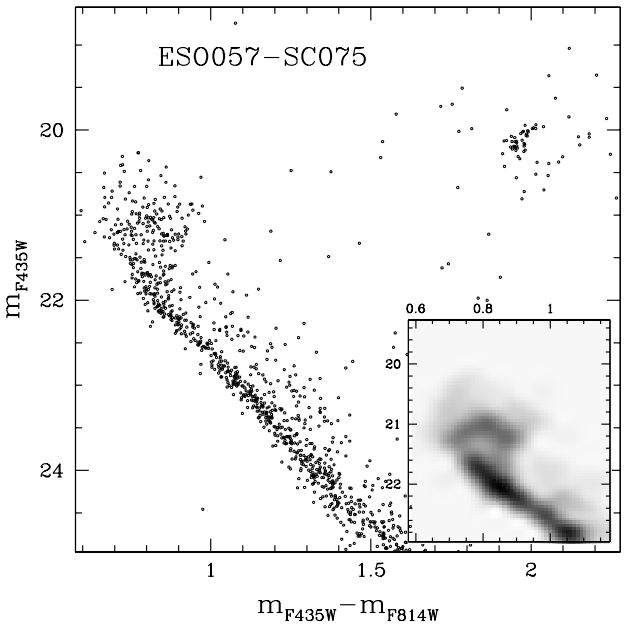

Fig. 12. As in Fig. 7 for ESO057-SC075.

The CMDs around the MSTO loci for the remaining twelve intermediate-age clusters that have been studied in this work are presented in Fig. 12 - 23.

Unfortunately, being this an archive project, the photometric data-set available for these twelve clusters is not homogeneous. One short and two deep images for each of the three filters: F435W, F555W, and F814W, were collected within pro-

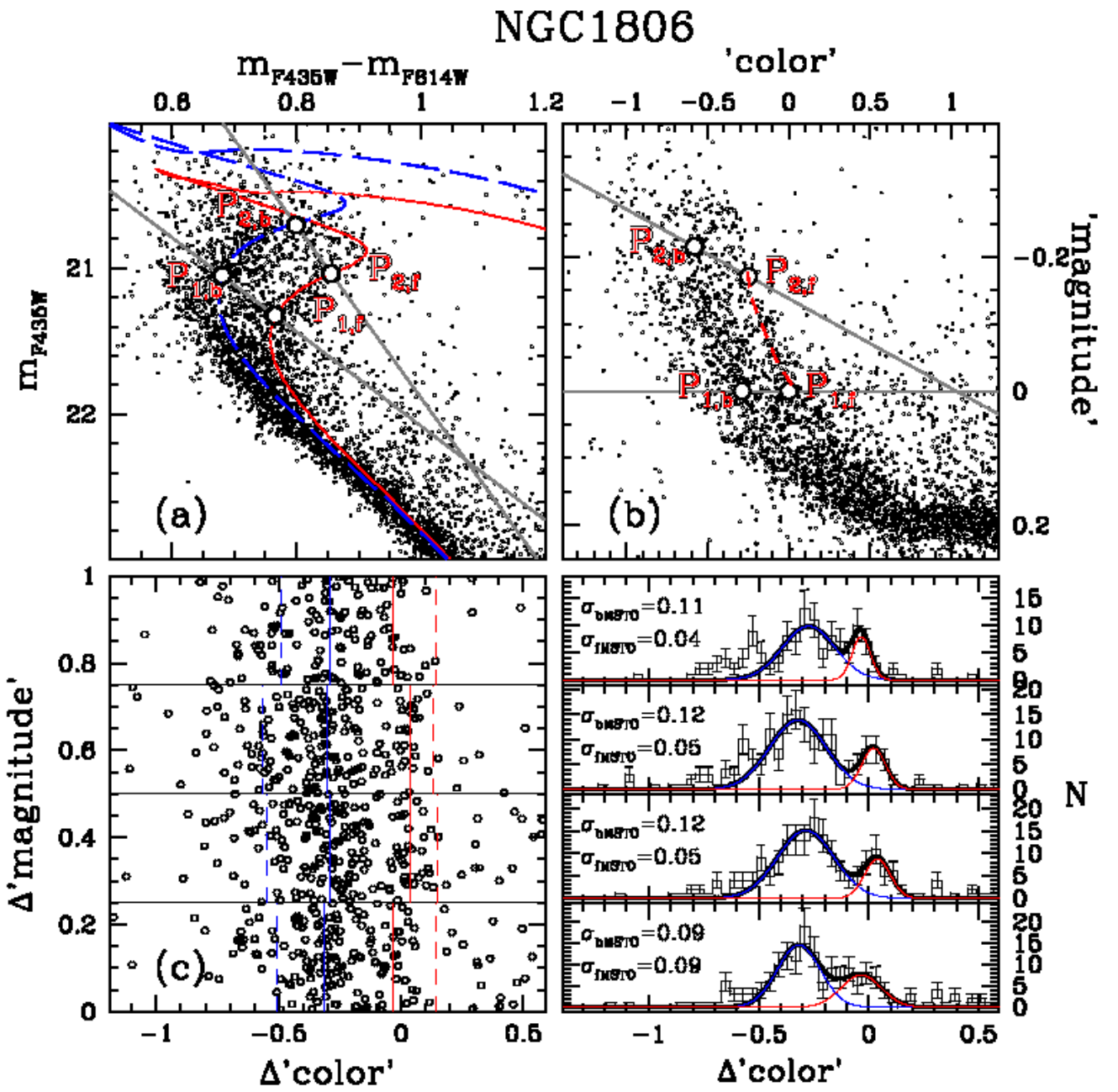

Fig. 10. This figure illustrates the procedure adopted to measure the fraction of stars belonging to the bMSTO and fMSTO in NGC 1806. Panel (a) shows a zoom of the CMD from Fig. 8 with the isochrones that best fits the fMSTO and the bMSTO overimposed. The grey lines delimit the portion of the CMD where the split is more evident. Only stars from this region are used to measure the population ratio. In Panel (b) we shifted and rotated the reference frame of Panel (a). Red dashed line is the fiducial of the region around the fMSTO. In Panel (c) we plotted stars between the grey lines but after the subtraction of the 'color' of the region around the fMSTO fiducial from the 'color' of each star and the division of the 'magnitude' of each star by the 'magnitude' of the upper grey line. The four right bottom panels show the Δ'color' distribution for stars in four Δ'magnitude' bins. The solid lines represent a bigaussian fit. For each bin, the dispersions of the best fitting gaussians are indicated.

gram GO 10595; while one single deep image in both F555W and F814W bands were collected within the snap-shot program GO 9891. Only two clusters were observed by both programs (NGC 1987 and NGC 2108), one cluster (ESO057-SC075) in GO-10595 only, and the remaining nine (HODGE 7, IC 2146, NGC 1644, NGC 1652, NGC 1795, NGC 1852, NGC 1917, NGC 1978 and NGC 2154) were observed within GO 9891 only (see Tab. 1 for more details).

We find that seven of these clusters show hints of an intrinsic spread around the MSTO: ESO057-SC075, HODGE 7,

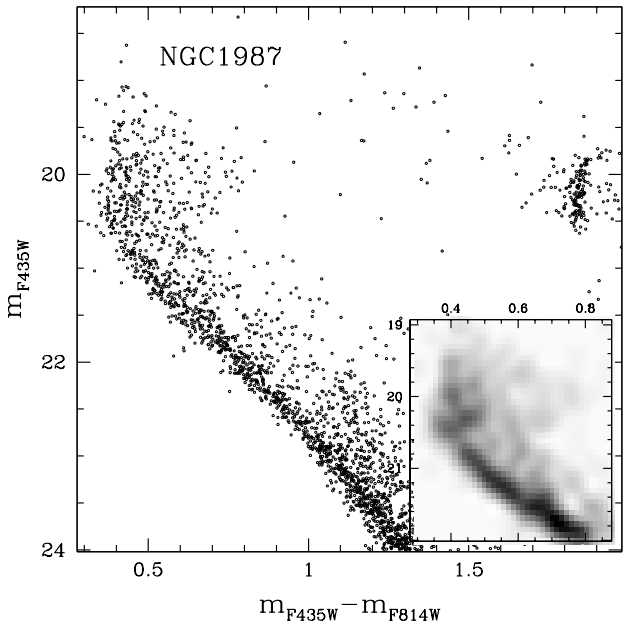

Fig. 13. As in Fig. 7 for NGC 1987.

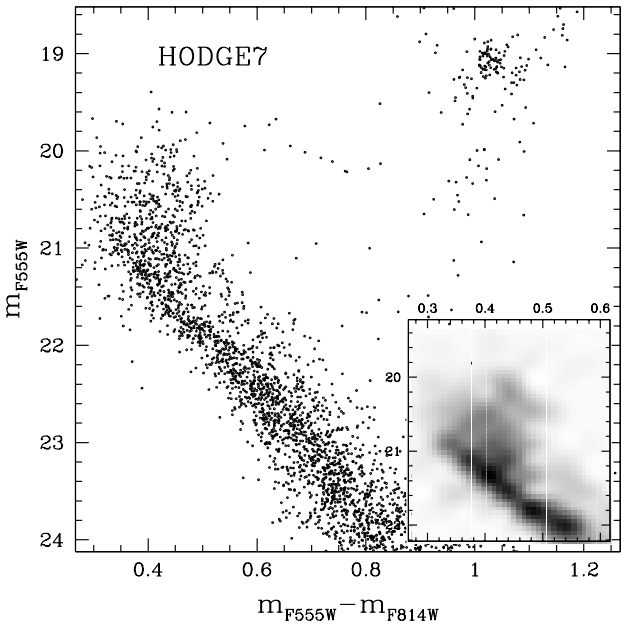

Fig. 15. As in Fig. 7 for HODGE 7.

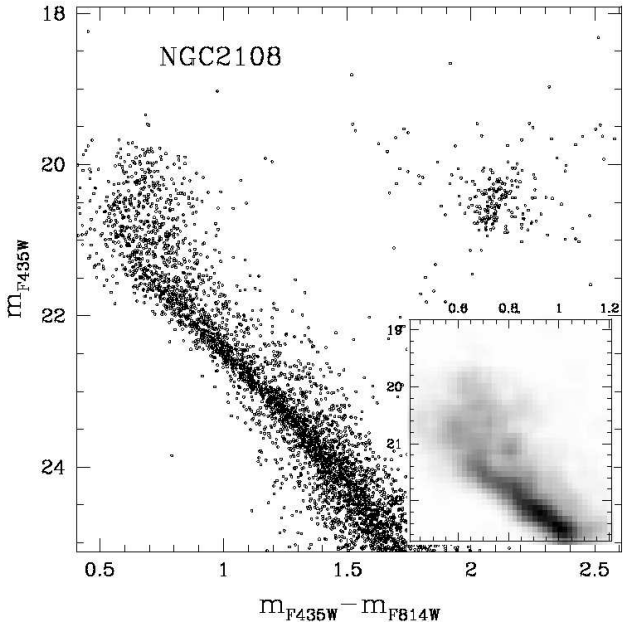

Fig. 14. As in Fig. 7 for NGC 2108.

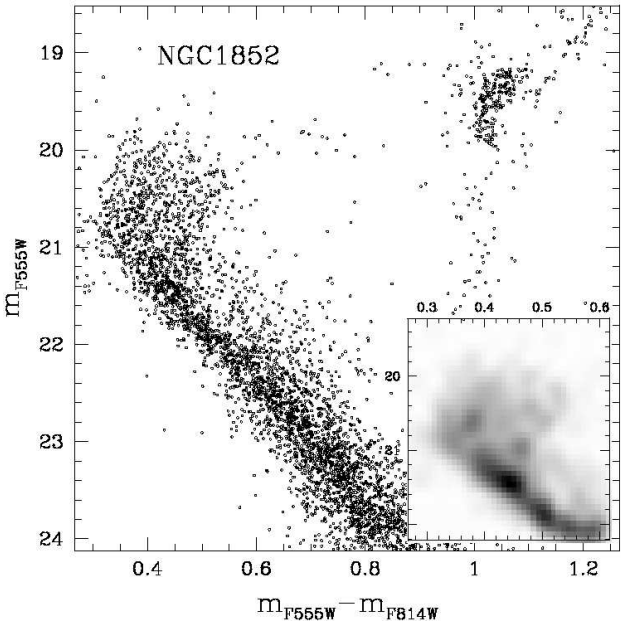

Fig. 16. As in Fig. 7 for NGC 1852.

NGC 1852, NGC 1917, NGC 1987, NGC 2108 and NGC 2154. The CMDs of IC 2146, NGC 1644, NGC 1652, NGC 1795 and NGC 1978 show no evidence for such a spread and are all consistent with hosting stars with the same age and chemical composition, within our photometric precisions. When simulated CMDs will be introduced, we will give a more objective criterion to discriminate clusters with an intrinsic spread around the MSTO (at the end of Section 6.2.2).

It must be noted that, apart from the broadened MSTO region, the other primary features of the CMDs of these clusters (MS, RGB and AGB) are narrow, and the HB red-clump is well-defined, thus the spread cannot be an artifact produced by differential reddening or variations of photometric zero points along the ACS field.

The limited statistic and photometric resolution do not allow us to establish wheter, these spreads are just unresolved splits –as those identified in the more populous clusters described in Sect. 4– or not.

In the following section, we show that the spread around the MSTO of the clusters mentioned above must be intrinsic. To do

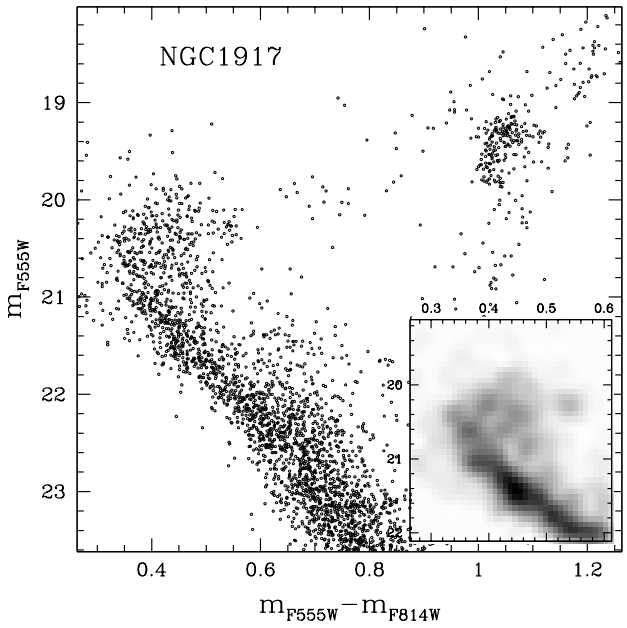

Fig. 17. As in Fig. 7 for NGC 1917.

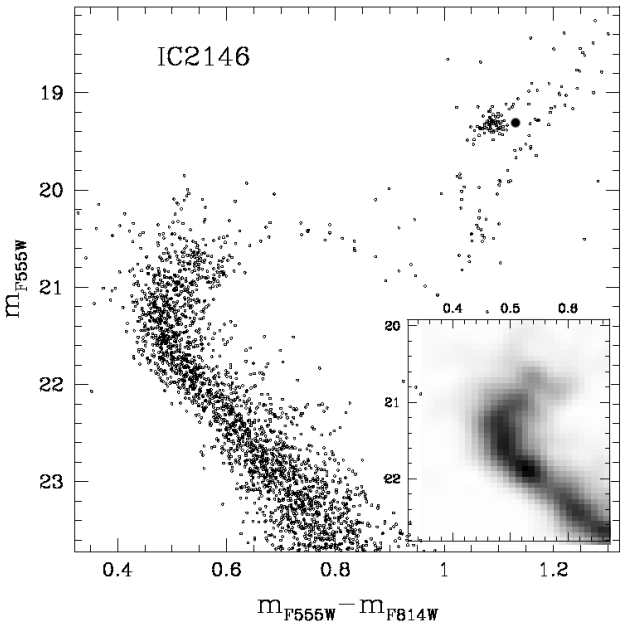

Fig. 19. As in Fig. 7 for IC 2146.

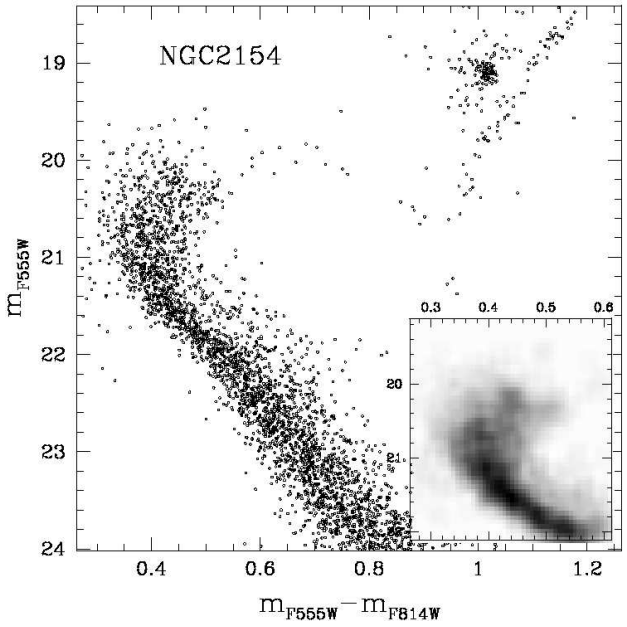

Fig. 18. As in Fig. 7 for NGC 2154.

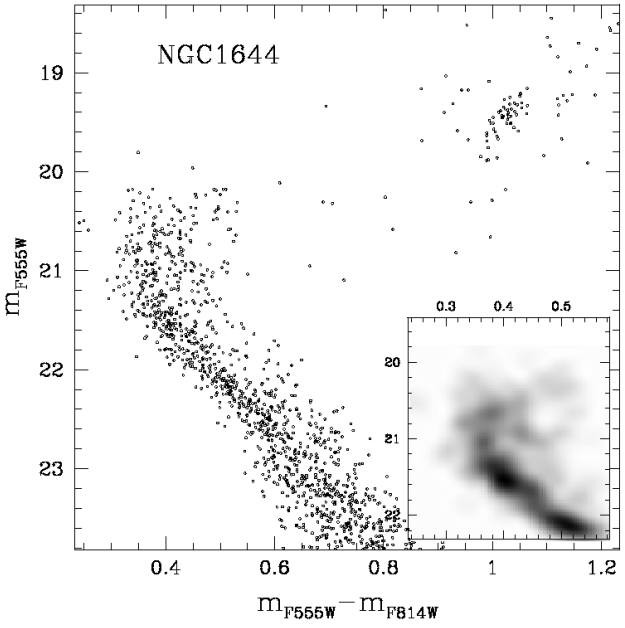

Fig. 20. As in Fig. 7 for NGC 1644.

this, we will demonstrate that the broadening we see cannot be explained by any combination of photometric errors, field-star contamination, or unresolved photometric binaries.

6. Does the spreaded MSTO reflect the presence of multiple stellar populations?

Globular-cluster systems with multiple populations manifest themselves in many different photometric ways. In ω Cen we (Anderson 1997, Bedin et al. 2004) have detected a split of the MS, which can only be explained by two stellar groups with different He content and metallicity (Piotto et al. 2005), and also at least four distinct SGBs (which may indicate age differences larger than 1 Gyr, see Villanova et al. 2007 and references within). In NGC 2808 we inferred the existence of three distinct stellar populations from the presence of three MSs (which is most easily explained by three groups of stars with different helium content, see Piotto et al. 2007). In the case of NGC 1851, the presence of two populations of stars is inferred from the fact that the SGB splits into two branches. This feature can be explained either by two distinct bursts of star formation with a

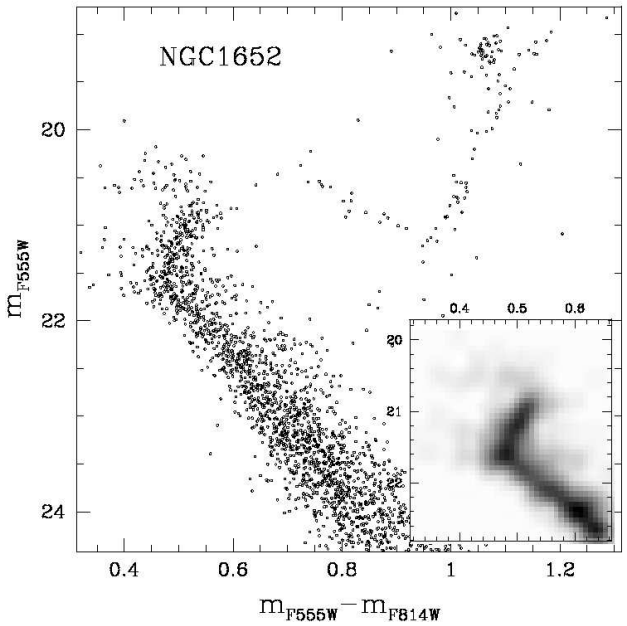

Fig. 21. As in Fig. 7 for NGC 1652.

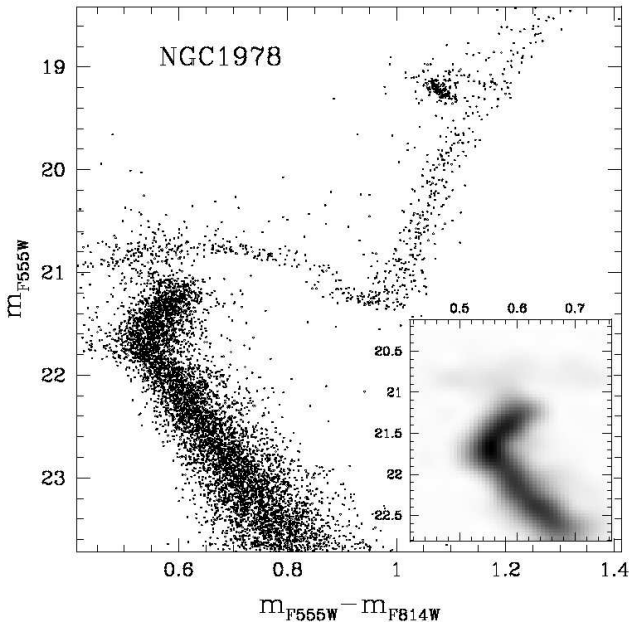

Fig. 23. As in Fig. 7 for NGC 1978.

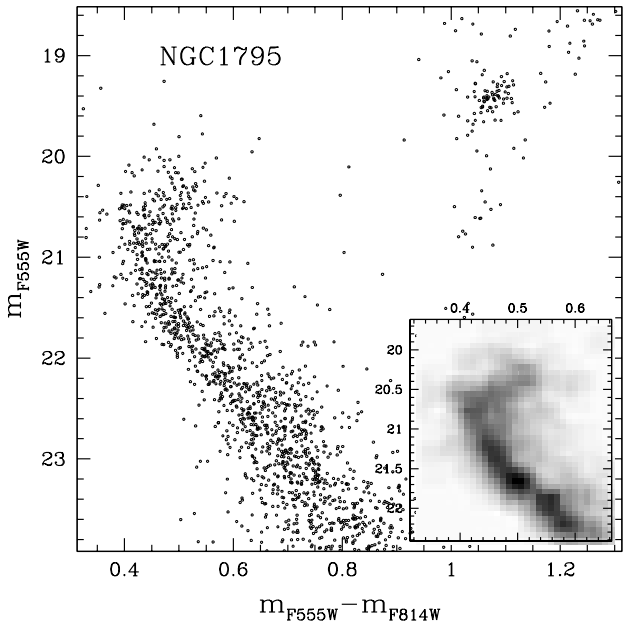

Fig. 22. As in Fig. 7 for NGC 1795.

time separation of about 1 Gyr, or by two stellar populations with distinct initial chemical composition and a much smaller age difference (Milone et al. 2008, Cassisi et al. 2008). A splits of the SGB have also been observed in NGC 6388 (Piotto 2008) demonstrating that this massive GC hosts two distinct stellar groups. In a spectro-photometric study of M4, Marino et al. (2008) detected a bimodal RGB, and demostrated that it is due to a bimodal distribution of CN, Na, O, indicating that also this relatively-small cluster contains multiple populations.

The Galactic clusters cited above variously exhibit broadening or bifurcation of the RGB, SGB, and lower MS populations. In the case of the intermediate-age LMC clusters we have studied here, we have detected both splits of the MSTO, as in NGC 1846 and NGC 1806 (Sec. 4, M07 and M08), in NGC 1751 and possibly NGC 1783 (Sec. 4), and a broadening of the MSTO as the clusters in Figs. 12 - 14 and NGC 2173 (Bertelli et al 2003). The low numbers of stars on the RGB make it difficult to assess the presence of a split or anomalous broadening along this evolutionary sequence, and the distance of the LMC makes it impossible to detect splits in the lower MS population with the presently available data.

While the splits and broadening we have shown above look quite convincing, it is important to consider the possibility that photometric errors or other effects can generate anomalous spreads and bifurcations, which could be confused with differences in age and/or chemical composition. In addition, it is also important to consider that both binaries and field stars contaminate the CMD region around the MSTO where we are most sensitive to the presence of multiple stellar populations.

In Section 6.1, we demonstrate that the MSTO broadening visible in Figs. 12- 14 is not due to field-star contamination by statistically subtracting field stars from the cluster CMD.

In Sec. 6.2, we consider the influence that binary stars could have on the spread of the MSTO. To do this, we will use artificial stars to simulate the CMD of a single population plus a population of binaries such that visible in the lower main sequence. We then present the decontaminated cluster CMD and compare it with the simulated one that includes both realistic errors and binaries to show that the observed MSTO broadening cannot be explained by a single population.

6.1. A method to decontaminate the cluster CMD from field stars

We began our analysis looking at the original CMD from stars near the cluster center, where we estimated that the contamination by field stars is at most at the level of ∼ 20% (see Section 3).

However, it is possible to reduce this contamination even further by doing a statistical subtraction of the stars that are most likely to be field stars. We have used the following approach which is based on the assumption that the distribution of field stars in the CMD of the cluster and reference field is nearly the same. For each star in the reference field CMD, we calculated the distance to all the cluster field stars: $d = \sqrt{(\Delta(m_{\rm F435W} - m_{\rm F814W}))^2 + (\Delta m_{\rm F435W})^2}$ (or $d = \sqrt{(\Delta(m_{\rm F555W} - m_{\rm F814W}))^2 + (\Delta m_{\rm F555W})^2}$), and flagged the closest cluster field star as a candidate to be subtracted. We remind to the reader that cluster and reference fields cover the same area.

We determined the ratio r between the completeness of this stars and the completeness of the reference field star. Note that this ratio is always $r < 1.0$. In order to avoid to over-subtract field stars, we generated a random number between 0 and 1, and removed the star from the cluster CMD if this random number was less than the ratio of the completenesses.

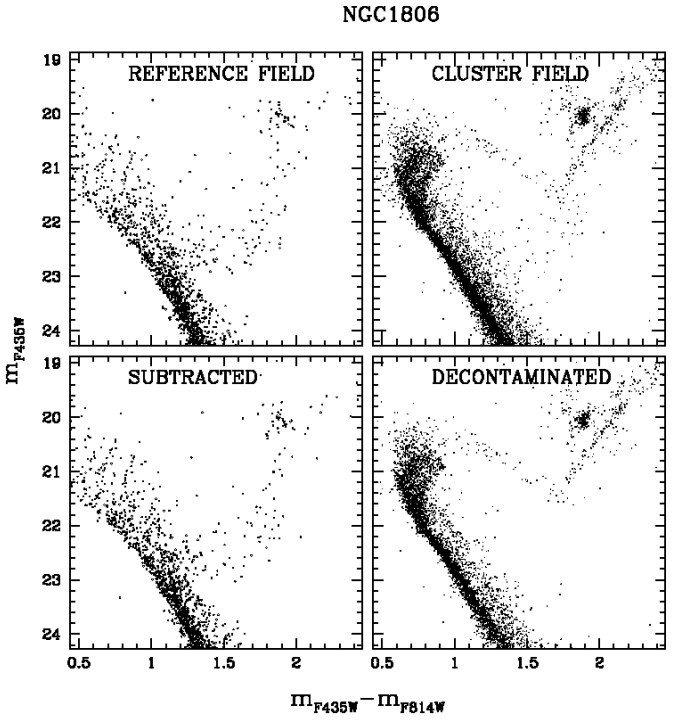

Fig. 24. Statistical decontamination from field stars of the CMD of NGC 1806. Upper panels: CMD extracted from the reference (left), and cluster fields (right). Bottom panels: CMD of all the stars that have been subtracted from the reference field (left) and decontaminated cluster CMD (right).

The main steps of this procedure are illustrated in Fig. 24 for NGC 1806: The upper panels show the CMD of stars in the reference (left) and cluster (right) field, the bottom ones the CMD of subtracted stars (left) and the decontaminated CMD (right). The statistical subtraction of field stars has not been applied to the most populated clusters (NGC 1978, NGC 1783), which occupy most of the field of view and have the highest ratio of cluster to reference field stars. We note that there is an additional young stellar cluster within the ACS images of NGC 1852, so we were careful to select a reference field that was as far as possible from both clusters.

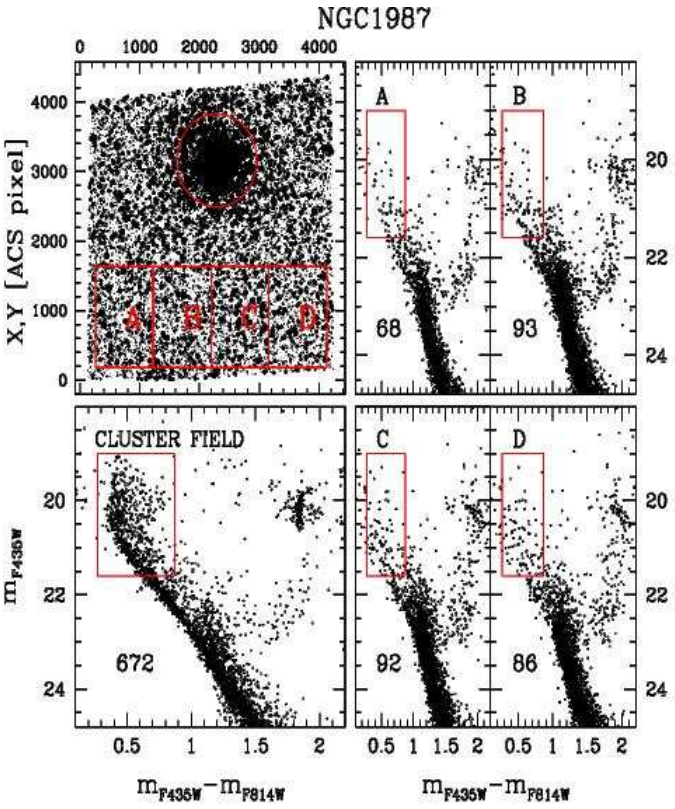

Fig. 25. Comparison of the CMD of the cluster field and those of four external reference regions (*A*, *B*, *C* and *D*) for NGC 1987. The values given in the bottom left corner of each CMD are the number of stars (corrected for incompleteness) in the box around the cluster MSTO.

Obviously, small variations in the distribution of stars in the reference field are expected even within the small WFC/ACS field of view. In order to check whether the reference field star distribution can be reasonably assumed uniform we defined four regions with the same area of the cluster field and the largest possible distance from the cluster center. We extracted the CMD of each region and compared it with that of the cluster field. A typical example of this procedure is shown in Fig. 25 for NGC 1987. In particular, we have compared the number of stars (corrected for completeness) in the boxed region around the MSTO. We found that, in most cases the variation of the number of stars in this region is smaller than about 30%. Obviously, this procedure has been applied only to clusters that cover a sufficiently small fraction of the ACS field of view. We cannot exclude that the variation of the number of

stars in reference field regions could be (partially) due to contamination of cluster members. However, we note that oversubtracting the cluster members does not affect our results on the morphology of the MSTO.

6.2. The synthetic CMD

The main goal of this section is to generate a synthetic CMD of a cluster with the same characteristics of the observed one, but hosting a single stellar population. This is a necessary step to demonstrate whether the observed spread in color around the MSTO is an intrinsic feature due to the presence of multiple stellar populations or an artifact produced by unresolved binaries or photometric errors.

In order to simulate a CMD that reproduces well enough the main properties of the observed one we must ensure that:

- the mass function of the synthetic CMD is as similar as possible to the observed one;
- simulated and observed stars have the same radial distribution, completeness, and photometric errors;
- the fraction and the mass ratio distribution of simulated photometric binaries are as close as possible to the real ones.

In the following we describe the procedure that we have used to generate a synthetic CMD with these requirements. It consists of two main steps: in the first one we generate single stars; in the second one we measure the fraction of photometric binaries in the observed CMD and add to the simulated CMD the corresponding number of binary systems.

6.2.1. Step one: simulation of single stars

We have separately simulated MS and evolved stars.

Unevolved Stars: To generate single MS stars we started by selecting a sub-sample of artificial stars with the following criterion. For each star in the cluster field that survive to the statistical subtraction of reference field stars of Section 6.1, we have assigned a sub-sample of the artificial stars and randomly extracted a star from it (see Sect. 2.2 for a description on how AS were generated). The artificial-star sub-sample consists of all the artificial stars with similar magnitudes (within 0.1 $m_{\rm F814W}$ mag) and radial distances (less then 50 pixel from the observed star). This method produces a catalog of simulated stars with almost the same luminosity, and radial distribution of the observed catalog. This procedure has been applied only to MS stars.

Evolved Stars: Things become more complicated for stars brighter than the MSTO where the complex shape of the CMD makes it harder to associate a star with the CMD sequence that corresponds to its evolutionary phase. For this reason, a different approach was used to simulate evolved stars (i.e. stars brighter than the MSTO).

First of all, we counted the number of MS stars (corrected for completeness) with $m^{\rm TO}_{\rm F814W} < m_{\rm F814W} < m^{\rm TO}_{\rm F814W} + 0.5$ and calculated the average number of stars per unit mass $N_{\mathcal{M}}$ in this range of luminosity. Next, we obtained $N_{\mathcal{M}}$ for stars brighter than the MSTO by using a Salpeter (1955) IMF and associated these stars to each portion of the CMD according to the Pietrinferni et al. (2004) models.

Since evolved stars should all have nearly the same mass, we would expect that they would also have the same radial distribution. For this reason, we randomly associated to each simulated evolved star the radial distance of an observed star brighter than the MSTO. Finally, for each simulated star, we selected the sample of artificial stars with almost the same magnitude, color and distance from the cluster center (we imposed that both input $m_{\rm F814W}$ magnitude and color must differ by less than 0.01 mag and radial distance by less than 50 pixels) and randomly extracted a star from it.

It must be noted that the simulated CMDs have photometric errors that are slightly smaller than the errors of real stars. This reflects a fundamental limitation of artificial-star tests: an artificial star is measured by using the same PSF that was used to generate it, while for the real stars we necessarely have an imperfect PSF. The PSF is constructed to fit the real stars as well as possible, but there will invariably be errors in the PSF model for the real stars, which will not be present for the artificial stars. [However, it must be clearly stated that these differences are appreciable only for the stars with the highest S/N ratio].

Below, we describe the method that we used to estimate the difference between the photometric errors of real and artificial stars. This allows us to introduce an additional error component to the artificial-star photometry so that the real and artificial sequences can be directly compared. We illustrate the procedure for the case of NGC 1806. The same procedure was applied for all clusters.

To determine how much artificial broadening of the error distribution is necessary, we compare the color distribution of the observed and simulated MS stars. Figure 26 shows the color distribution of MS stars for NGC 1806: the left panel contains the CMD of all the stars contained in the cluster field after the subtraction of the reference field stars. The red fiducial line (MSRL) is computed by using the following procedure. We started by dividing the CMD into bins of magnitude in the F814W band and, for each bin, we calculated the median color and magnitude and obtained a raw fiducial line by fitting these points with a spline. Then we derived for each star the absolute value of the difference between its color and the color of the fiducial line, and calculated the σ as the $68.27^{\rm th}$ percentile. All the stars with distances larger than $N\,\sigma$ from the fiducial were rejected and the survivors used to redetermine the median color, magnitude and σ. We iterated this procedure five times with N going from 6 to 2 (integer numbers).

In the middle panel we show the straightened CMD obtained by subtracting from the color of each star the color of the fiducial line. In the right panel we show the histograms of the color distribution in eight $m_{\rm F814W}$ magnitude intervals. The distribution in color is well reproduced by a Gaussian plus a tail on the red side due to the conspicuous number of photometric binaries and blends.

In Fig. 27 we also reproduce the distribution in color for the artificial star MS. As expected, the spread of the latter is slightly lower than that of the observed MS. We note that the

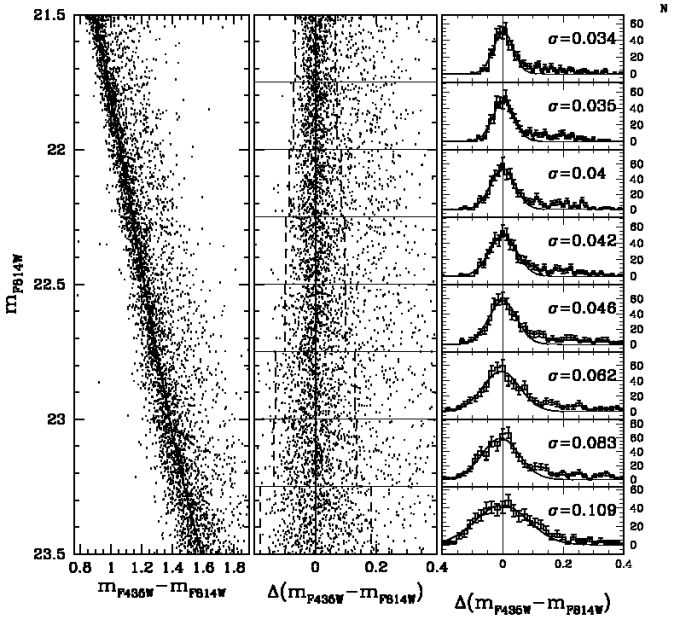

Fig. 26. *Left* : CMD of NGC 1806 with the MSRL overplotted; *Middle* : The CMD rectified by subtraction of the MSRL; *Right* : Color distribution of the rectified CMD. The σ in the inset are those of the best-fitting gaussians.

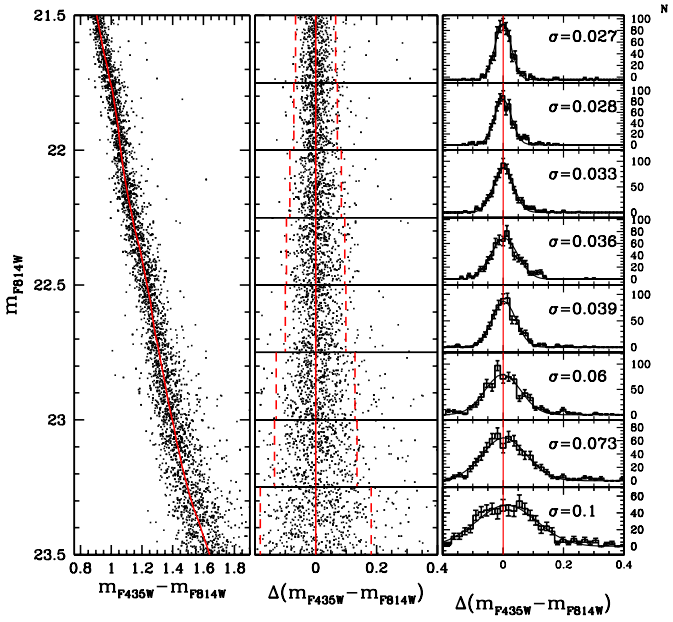

Fig. 27. As in Fig. 26 but for artificial stars

presence of this additional dispersion, does not allow us to exclude intrinsic dispersion of the MSs smaller than 0.03 mag in color, which might result from dispersion of Z, Y, or a combination of the two (see discussion in Milone et al. 2008). In Fig. 28 we compare the dispersions of the observed MS ($\sigma_{\rm OBS}$, circles) and for artificial stars ($\sigma_{\rm ART}$, triangles) as a function of

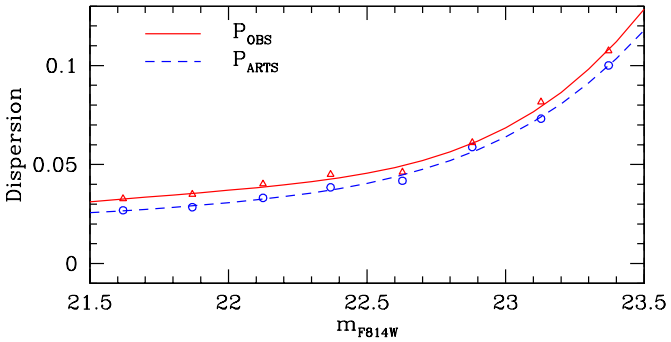

Fig. 28. Comparison of the σ of gaussians that best fit the color distributions of MS stars in the observed (red triangles) and artificial stars (blue circles) CMD as a function of the $m_{\rm F814W}$ magnitude. Continuous and dashed lines are the best fitting fourth order polynomials.

the $m_{\rm F814W}$ magnitude; the continuous lines are the best fitting fourth order polynomials ($P_{\rm OBS}$ and $P_{\rm ART}$). Finally, we added to the color of each star of the artificial-star CMD an error randomly extracted from a Gaussian distribution with dispersion $P_{\rm DIF} = \sqrt{P^2_{\rm OBS} - P^2_{\rm ART}}$.

6.2.2. Step two: simulation of binary systems

It is clear from the excess of stars on the red side of the main sequence that many of these clusters have a sizeable binary populations (compare Fig. 26 with Fig. 27). We expect that this binary population can have some effect on the distribution of stars around the turnoff, so we will estimate the binary-contamination effect. Binary stars of LMC clusters will be unresolved even with *HST*, but the light from each star will combine and the binary system will appear as a single point-source object. These binaries can be discerned photometrically from the single stars along the MS as they are located brightward and to the red of the sequence. The position of the binary systems formed by two MS stars (MS-MS binaries) with a different mass ratios in a typical CMD of an intermediate age LMC clusters are illustrated in Fig. 29.

In the same region of the CMD, in addition to the true physically associated binaries, we expect also a few chance superpositions (blends). The artificial-star tests (see Fig. 27) show that this is a very small effect.

It is important to note here that measuring the fraction of binaries is not the goal of this paper; our aim here is to estimate their fraction so that we can determine how much of the spread of the MSTO region can reasonably be attributed to them.

Binaries can be parametrized by their mass ratio, $q = m_1/m_2$, where $m_1 < m_2$. In order to estimate the fraction of MS-MS photometric binaries with mass ratio greater than a threshold value (hereafter $q_{\rm th}$, see Tab. 2 for the adopted $q_{\rm th}$ for each cluster) we have applied the methods described in Milone et al. (2008) and Bedin et al. (2008). We divided the CMD into two regions: the first one (A) contains all the single MS stars and binaries with a primary star with $(m^{\rm MSTO}_{\rm F814W} + 0.4) < m_{\rm (F814W)} < (m^{\rm MSTO}_{\rm F814W} + 2.4)$ (where $m^{\rm MSTO}_{\rm F814W}$ is the magnitude of the MSTO in

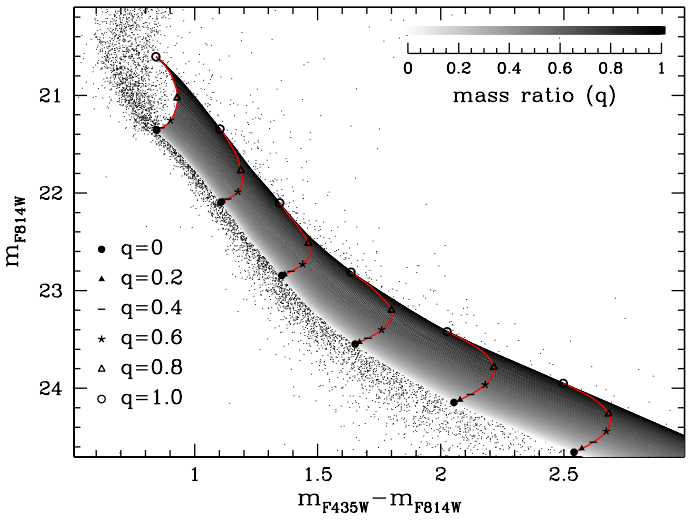

Fig. 29. Grey area highlight the loci populated by MS-MS binaries. The levels of grey are proportional to the mass ratio. Red lines indicate the position of a MS-MS binary for six fixed values of the mass of the primary star (m_1) and q ranging from 0 to 1.

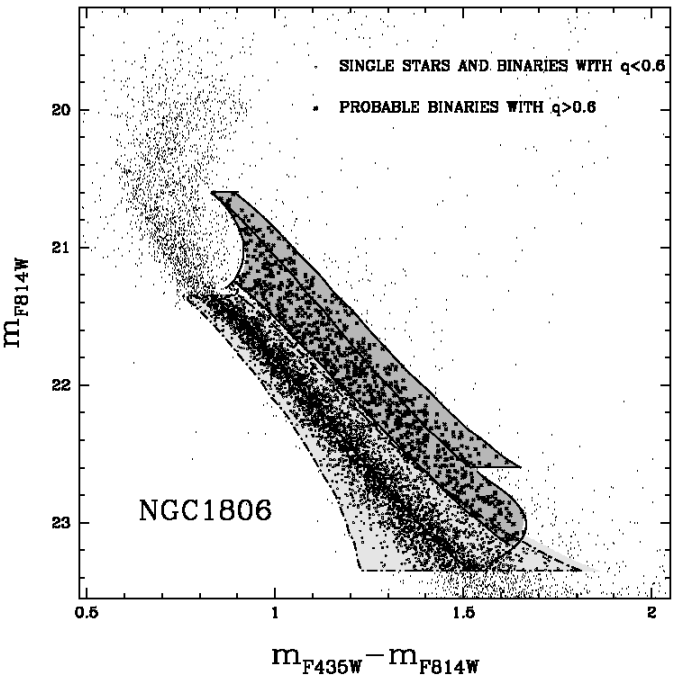

Fig. 30. The MS of NGC 1806 with the candidate binaries with mass ratio $q > 0.6$ plotted as crosses.

the F814W band). It corresponds to the light and dark grey area of Fig. 30. The second region (*B*) is the part of *A* that contains MS-MS binaries with $q > q_{\rm th}$, and corresponds to the dark grey area of Fig. 30. We adopted $q_{\rm th} = 0.6$ or $q_{\rm th} = 0.7$, as indicated in Tab. 2, depending on the photometric quality of the data. The fraction of binaries with $q > q_{\rm th}$ has been evaluated as:

$$f_{\rm BIN}^{q>q_{\rm th}} = \frac{N^{\rm B}_{\rm CLUSTER} - N^{\rm B}_{\rm REFERENCE}}{N^{\rm A}_{\rm CLUSTER} - N^{\rm A}_{\rm REFERENCE}} - \frac{N^{\rm B}_{\rm ARTS}}{N^{\rm A}_{\rm ARTS}}$$

Where $N^{\rm A(B)}_{\rm CLUSTER}$ is the number of stars (corrected for completeness) observed in the region A (B) of the CMD extracted from the cluster field. $N^{\rm A(B)}_{\rm REFERENCE}$ are the corresponding numbers of stars in the CMD of the reference field and account for the field contamination. $N^{\rm A(B)}_{\rm ARTS}$ refer to artificial stars: their ratio indicates the fraction of blends. Finally, we calculated the global fraction of binaries by interpolation, assuming a flat mass-ratio distribution. The only differences from what done in Milone et al. (2008) and Bedin et al. (2008) is that in this paper we have removed the contribution from field stars by using the CMD observed in the reference region, rather than by using a Galactic model or proper motions. The measured fraction of binaries in each cluster are in Tab. 2.

We tried very hard to get a reliable binary fraction for those clusters, but unfortunately, their are just too big on ACS/WFC FOV. If we take the outskirts as representative of the field we would end up subtracting cluster members from clusters, and since energy equipartion make the binary to sink into the cluster core, this could potentially generate dangerous biases in the relative fraction of single to binary system. We avoid on purpose to give numbers in Table 1 for those clusters, to avoid contamination of the literature with unreliable values of the binary-fraction for those objects.

To simulate binary stars to be added to the simulated CMD described in Sec. 6.2 we adopted the following procedure:

ID	$q_{\rm th}$	$f_{\rm bin}^{q>q_{\rm th}}$	$f_{\rm bin}^{\rm TOT}$
ESO057-SC075	0.6	0.17±0.02	0.42±0.05
HODGE7	0.7	0.08±0.01	0.27±0.04
NGC1644	0.7	0.09±0.02	0.29±0.06
NGC1652	0.7	0.06±0.01	0.19±0.04
NGC1751	0.6	0.13±0.01	0.33±0.03
NGC1795	0.7	0.12±0.02	0.39±0.06
NGC1806	0.6	0.13±0.01	0.32±0.03
NGC1852	0.7	0.11±0.02	0.36±0.05
NGC1917	0.7	0.09±0.02	0.31±0.05
NGC1987	0.6	0.12±0.01	0.31±0.03
NGC2108	0.6	0.18±0.01	0.46±0.03
NGC2154	0.7	0.08±0.01	0.28±0.04

Table 2. Fraction of photometric binaries with $q > q_{\rm th}$ and total fraction of binaries (columns 5 and 6) within the cluster field.

- We selected a fraction $F_{\rm BIN}$ of single stars equal to the measured fraction of binaries and derived their masses by using the Pietrinferni et al. (2004) mass-luminosity relation (for the clusters where the measure of the binary fraction is not available we assumed the average value of $F_{\rm BIN} = 0.33$);
- For each of them, we calculated the mass $\mathcal{M}_2 = q \times \mathcal{M}_1$ of the secondary star and obtained the corresponding $m_{\rm F814W}$ magnitude. Its color was derived by the MSRL;
- Finally, we summed up the F435W (or F555W) and F814W fluxes of the two components, calculated the corresponding magnitudes, added the corresponding photometric error, and replaced in the CMD the original star with this binary system.

Figures 31, 32, 33 and 34 show the contribution that we would expect from binaries to the broadening of the cluster TOs. It is clear that the double MSTO in NGC 1806, NGC 1846, and NGC 1751, and the extended (broadened) MSTO in ESO057-SC075, HODGE 7, NGC 1783, NGC 1852, NGC 1917, NGC 1987, NGC 2108 and NGC 2154 are intrinsic features of these objects, and cannot due to field-star contamination, photometric errors or binaries. In these figures, we show, from the left to the right, a zoom of the original cluster-field CMD around the MSTO, the same portion of the CMD but for stars in the reference field, the CMD after field-star decontamination, and the simulated CMD for these clusters.

Figure 35 and 36 illustrate the same exercise for the clusters with no significant MSTO broadening. Now that we have introduced the simulated CMDs we can describe how we discriminate between clusters that show evidence of hosting a multiple population, and those which do not. First, we calculated the dispersion of stars along a same direction perpendicular to the obseverd spread (on the right of the MSTO) for real (σ_{SGB}^{OBS}) and artificial stars (σ_{SGB}^{ART}). Then, we considered a cluster as hosting a multiple population if the dispersion of real stars was more than three times the dispersion of the simulated CMD. This condition is verified for eleven out the sixteen clusters. Although the exact position of the line along which to measure the spread is not unique, it seemed to us a reasonably solid approach.

7. Isochrones fitting

M07 and M08 proposed that the split of the MSTO of NGC 1846 and NGC 1806 is consistent with the presence of two distinct stellar populations with the same chemical composition and a difference in age of about $\sim$ 300 Myr. In addition, M08 have suggested that the spread of the MSTO of NGC 1783 can be attributed to a prolonged star formation.

In the previous sections, we have demonstrated that eight additional clusters show strong indications of an intrinsic spread or split of the CMD around the MSTO region. The remaining five objects of our sample show no significant evidence for multiple stellar population within our photometric precision (see Fig. 35 and 36).

We note that in the clusters where a spread in the MSTO is claimed, the other evolutionary sequences are narrow and well defined, after a correction for differential reddening has been made. The tightness of these other sequences is also a strong indication that there is very little variation in metallicity among the stars.

Therefore, in the absence of any detailed chemical composition analysis, in what follows we will assume that any spread around the MSTO can be attributed to a difference in age alone. We will derive the main parameters for each cluster (metallicity, age, and the maximum age spread among the populations) by fitting the data with the isochrones from the BaSTI evolutionary code (Pietrinferni et al. 2004, updated version of August 2008). Each of the isochrones has a solar-scaled distribution of metals and includes convective overshooting.

To determine the isochrone that best matches the observed CMD of our clusters with no evidence of an intrinsic spread around the MSTO we followed a procedure similar to the one adopted by M07. We generated a grid of isochrones using metallicities of Z= 0.008 and 0.010, sampling an age range between 1.0 and 3.0 Gyrs at intervals of 0.05 Gyr. Then, we defined by hand: the magnitude of the MSTO, the color of the RGB at a level intermediate between that of the red end of the SGB and that of the HB red-clump, and the magnitude of the HB red-clump. In this way we calculated the difference in magnitude between the MSTO and the HB red-clump ($\Delta_{\rm mag}$) and the difference in color between the MSTO and the fiducial points on the RGB ($\Delta_{\rm col}$). Then we calculated a value of $\Delta_{\rm mag}$ and $\Delta_{\rm col}$ for each isochrone in the grid and compared them with the observed ones. Finally, we selected all the isochrones where $\Delta_{\rm col}$ and $\Delta_{\rm mag}$ differ respectively by less $\pm$0.25 and $\pm$0.03 magnitudes and fitted them to the CMD by hand. To do this, we varied the distance modulus in the range $18.30 < (m-M)_0 < 18.70$ and the reddening between 0.00 and 0.30, both in steps of 0.01 mag and searched for the combination that best matches the cluster sequences. For clusters with a double or broadened MSTO, we used a similar approach with the exception that, in this case, we first defined on the observed CMD the magnitude of the MSTO and the values of $\Delta_{\rm mag}$ and $\Delta_{\rm col}$ for the bMSTO and determined the isochrone that best fits this younger population. Then, we selected all the isochrones with the same metallicity, distance modulus and reddening, but different ages and fitted the fMSTO (for clusters with a broadened MSTO we calculated those values that correspond to the brighter and the fainter region of the MSTO).

The best fitting distance modulus, reddening, metallicity and age are listed in Tab. 3. The last column indicates the maximum age difference, $\Delta_{\rm age}$, for stars in clusters that show possible evidence of multiple or prolonged star formation episodes.

ID	$(m-M)_0$	$E(B-V)$	Z	Age (Myr)	$\Delta_{\rm age}$
ESO057-SC075	18.46	0.14	0.008	1400-1600	200 ± 50
HODGE7	18.48	0.04	0.008	1400-1550	150 ± 50
IC2146	18.50	0.07	0.008	1550	< 50
NGC1644	18.48	0.01	0.008	1550	< 50
NGC1652	18.48	0.06	0.008	1700	< 50
NGC1751	18.45	0.22	0.008	1300-1500	200 ± 50
NGC1783	18.46	0.06	0.008	1400-1600	200 ± 50
NGC1795	18.45	0.10	0.008	1300	< 50
NGC1806	18.44	0.09	0.008	1400-1600	200 ± 50
NGC1846	18.49	0.09	0.008	1350-1600	250 ± 50
NGC1852	18.50	0.08	0.008	1200-1450	250 ± 50
NGC1917	18.48	0.08	0.008	1200-1350	150 ± 50
NGC1978	18.49	0.09	0.008	2000	< 100
NGC1987	18.40	0.04	0.010	950-1200	250 ± 50
NGC2108	18.40	0.21	0.010	950-1100	150 ± 50
NGC2154	18.48	0.04	0.008	1350-1500	150 ± 50

Table 3. Parameters that have been used to obtain the best fit between the observed CMD and the BaSTI isochrones.

In Fig. 37, Fig. 38 and Fig. 39, we have overplotted to the observed CMDs the best fitting isochrones. Interestingly, the multiple (or prolonged) star-formation episodes seem to lay between 150 and 250 Myr, very similar to the time interval between successive star formation episodes in the intermediate mass AGB star ejecta pollution depicted by Ventura et al (2001).

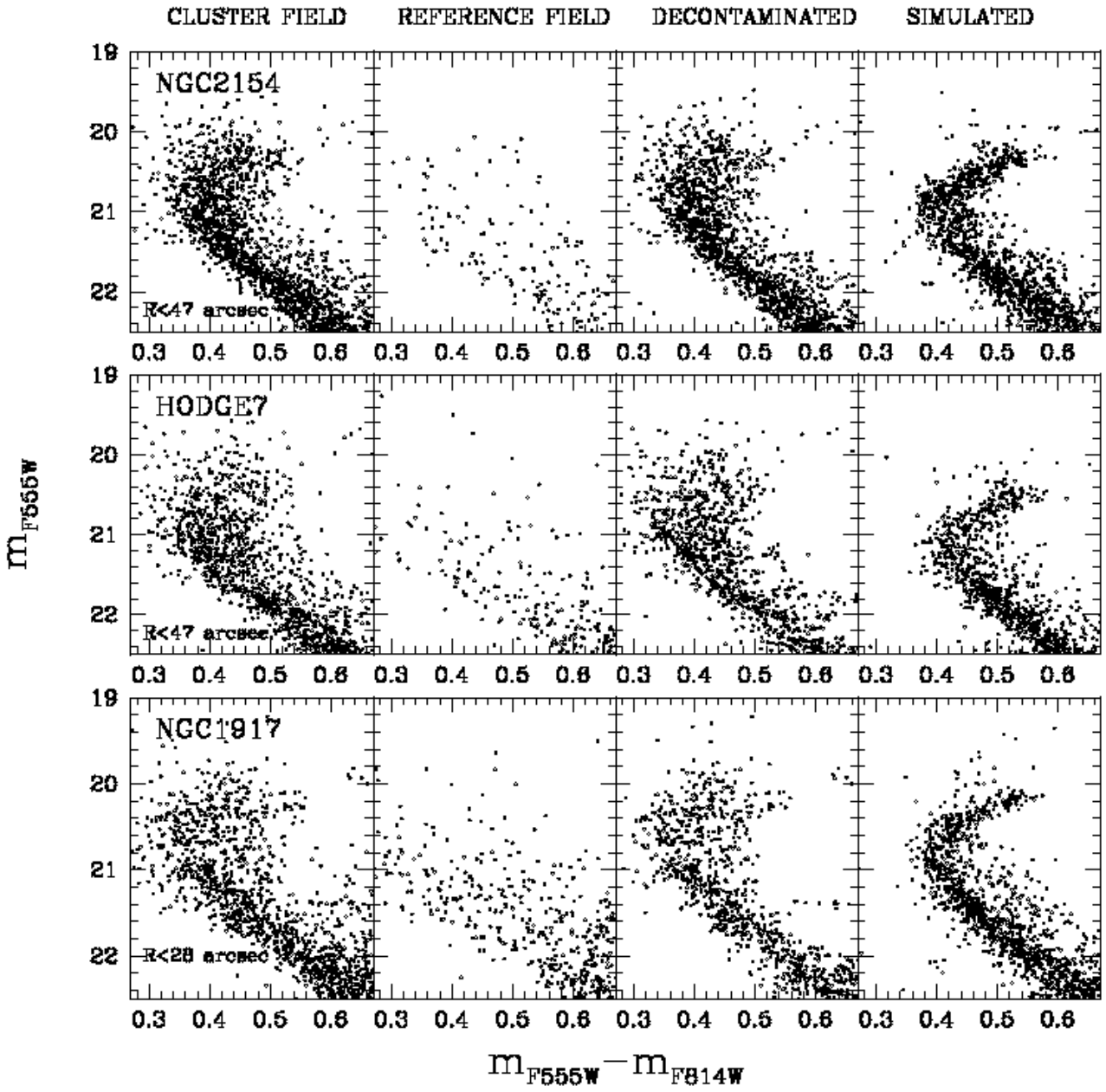

Fig. 31. From the left to the right: CMD of the cluster field for NGC 2154, HODGE 7 and NGC 1917, CMD of the reference field, CMD of the cluster field after that reference field stars have been statistically subtracted, simulated CMD.

8. Conclusions

High precision *HST* ACS/*HST* photometry of sixteen intermediate age LMC stellar clusters has revealed that eleven of them (i.e. about the 70±25% of the entire sample) host multiple stellar populations.

The CMDs of NGC 1806, NGC 1846 and NGC 1751 exhibit two dinstinct MSTOs, suggesting that these clusters have experienced (at least) two main episodes of star formation with a temporal separation of 200 - 250 Myr. For these three clusters the high quality of our photometry enabled us, not only to distinguish the two populations, but also to measure the fraction of stars belonging to each of them. In all the cases, the population corresponding to the brighter MSTO (the younger population) is the main population, and includes more then two-third of cluster stellar population, consistent with the intermediate mass AGB pollution scenario (See D'Antona & Caloi 2008 for a recent review).

Our photometry strongly suggests that the intrinsic broadening of the MSTO of NGC 1783 observed by M08 could be attributed to the presence of two distinct branches which are closely spaced and poorly resolved by the observations.

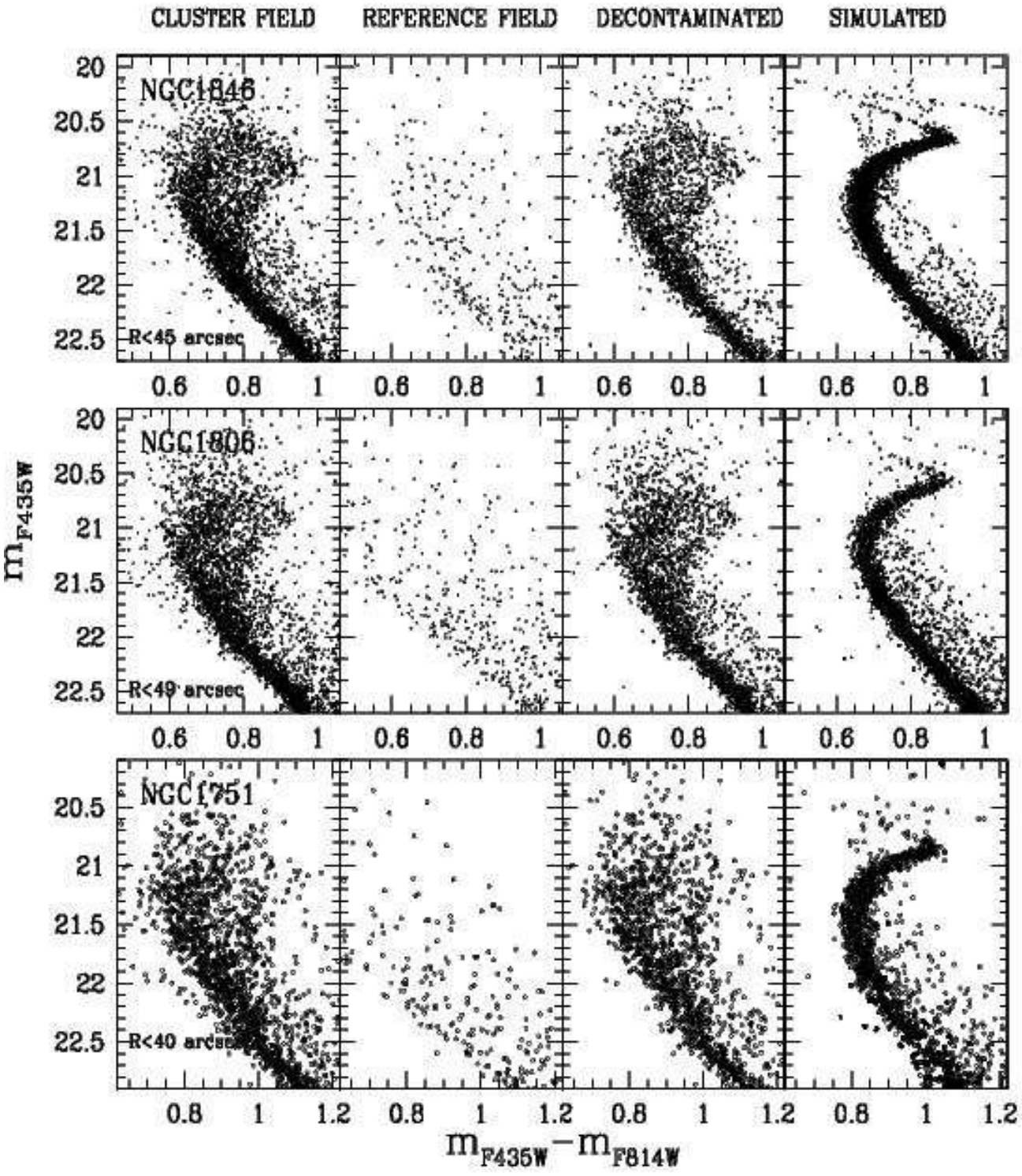

Fig. 32. As in Fig. 31 for NGC 1846, NGC 1806 and NGC 1751.

In seven additional clusters, namely ESO057-SC075, HODGE7, NGC 1852, NGC 1917, NGC 1987, NGC 2108, and NGC 2154 we observed a wide spread in color for the stars around the MSTO. In spite of this, the other main features of the CMD are narrow and well-defined, demonstrating that the spread cannot be an artifact produced by differential reddening, by variation of the photometric zero point along the chip, or by a relatively large spread in metallicity. By using the CMD of the stars in the fields that surround the cluster, we demonstrate that the observed feature is unequivocally associated with the clusters. Finally, artificial stars and simulated CMDs show that the wide spread in color observed around the MSTO cannot be

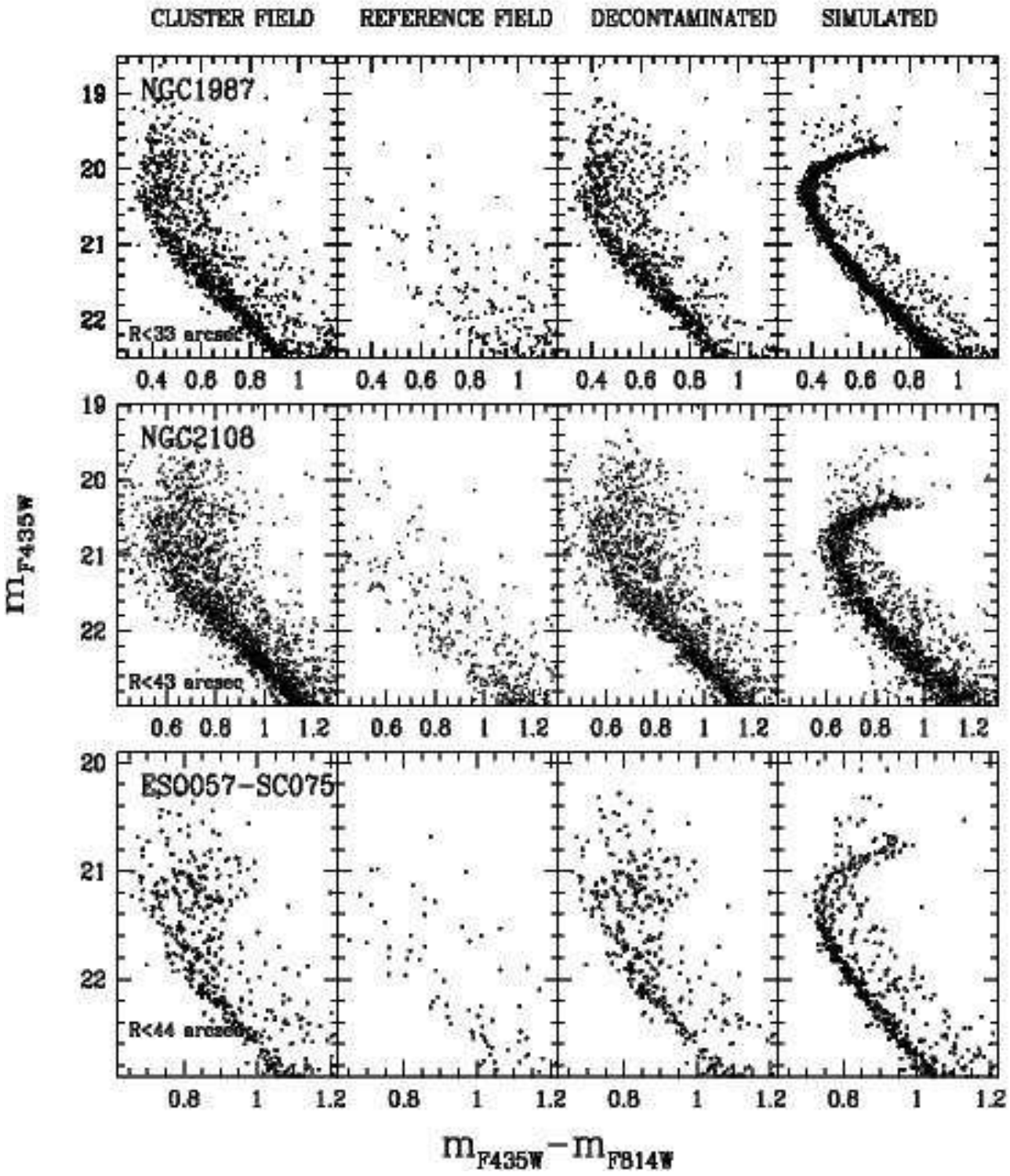

Fig. 33. As in Fig. 31 for NGC 1987, NGC 2108 and ESO057-SC075.

produced by photometric errors or binaries. It is interesting to note that the age spreads observed in this sample appear to be quite similar: they are all between 150 and 250 Myr.

Acknowledgements. We thank the anonymous referee for the careful reading of the manuscript, and for the useful comments.

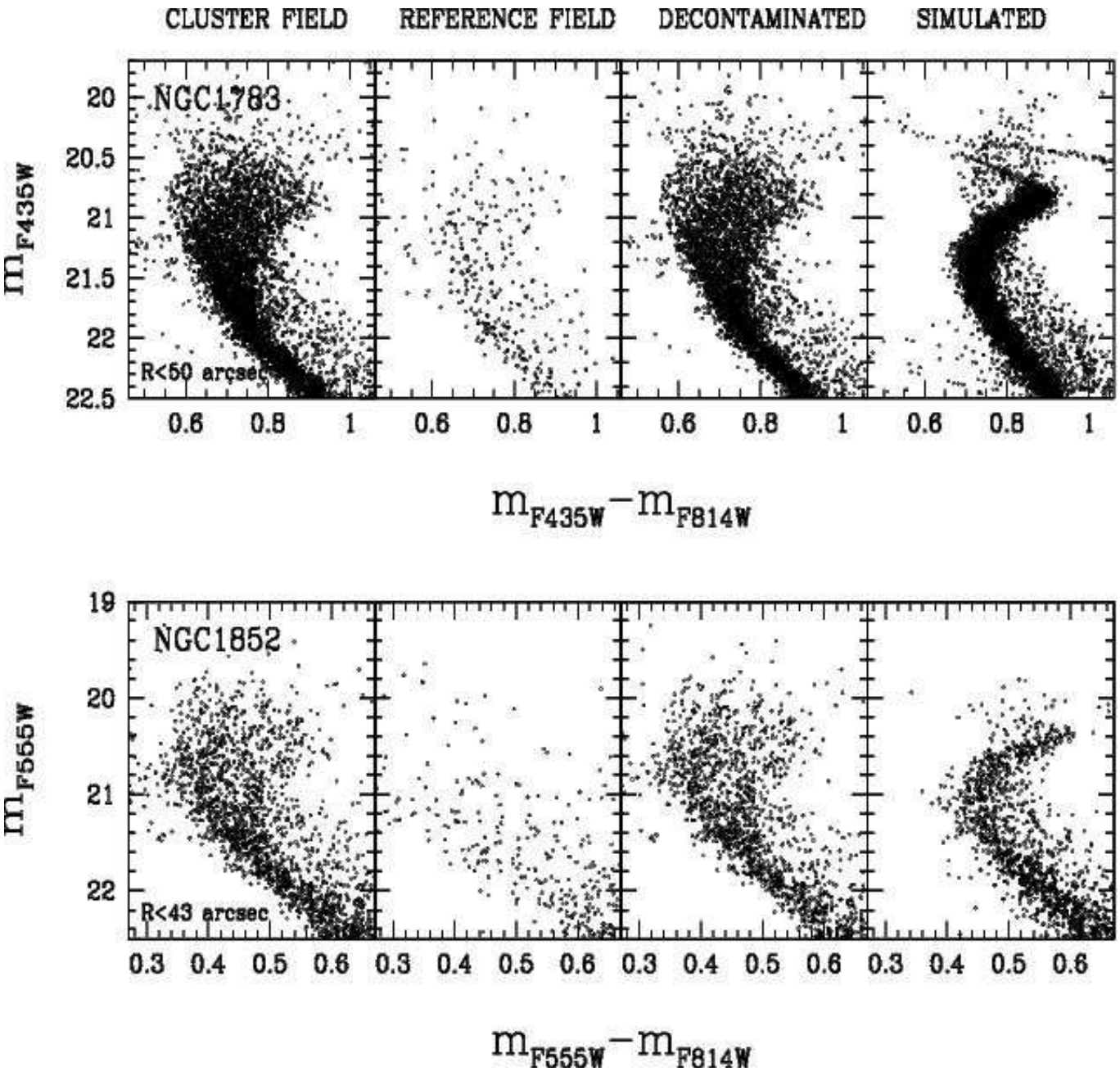

Fig. 34. As in Fig. 31 for NGC 1783 and NGC 1852.

References

Anderson, J. 1997, Ph.D. thesis, Univ. California, Berkeley

Anderson, J. & King, I. R., 2006. ACS/ISR 2006-01, PSFs, Photometry and Astrometry for the ACS/WFC

Anderson, J. et al. 2008, AJ, 135, 2055

Bedin, L. R., Piotto, G., Anderson, J., Cassisi, S., King, I. R., Momany, Y., & Carraro, G., 2004, ApJ, 605, L125

Bedin, L. R., Cassisi, S., Castelli, F., Piotto, G., Anderson, J., Salaris, M., Momany, Y. & Pietrinferni, A., 2005, MNRAS, 357, 1048

Bedin, L. R., Salaris, M., Piotto, G., Cassisi, S., Milone, A. P., Anderson, J., & King, I. R., 2008, ApJ, 679, L29

Bertelli, G. Nasi, E., Girardi, L., Chiosi, C., Zoccali, M., & Gallart, C. 2003, AJ, 125, 770

Cassisi, S., Salaris, M., Pietrinferni, A., Piotto, G., Milone, A. P., Bedin, L. R., & Anderson, J., 2008, ApJ, 672, L115

D'Antona, F., Bellazini, M., Caloi, V., Fusi Pecci, F., Galleti. S., & Rood, R. T., 2005, ApJ, 631, 868

D'Antona, F., & Caloi, V., 2008, accepted for publication in MNRAS (arXiv:0807.4233)

Glatt, K., et al. 2008a, AJ, 136, 1703

Glatt, K., et al. 2008b, AJ, 135, 1106

Gratton, R. G., et al. 2001, A&A, 369, 87

Gratton, R. G., Sneden, C., & Carretta, E. 2004, ARA&A, 42, 385

Mackey, A. D., & Broby Nielsen, P. 2007, MNRAS, 369, 921 (M07)

Mackey, A. D., Broby Nielsen, P., Ferguson, M. N. & Richardson, J. C. 2008, ApJ, 681, 17L (M08)

Marino, A. F., Villanova, S., Piotto, G., Milone, A. P., Momany, Y., Bedin, L. R., & Medling, A. M., 2008, accepted for pubblication in A&A (arXiv:0808.1414)

Milone, A. P. et al. 2008, ApJ, 673, 241

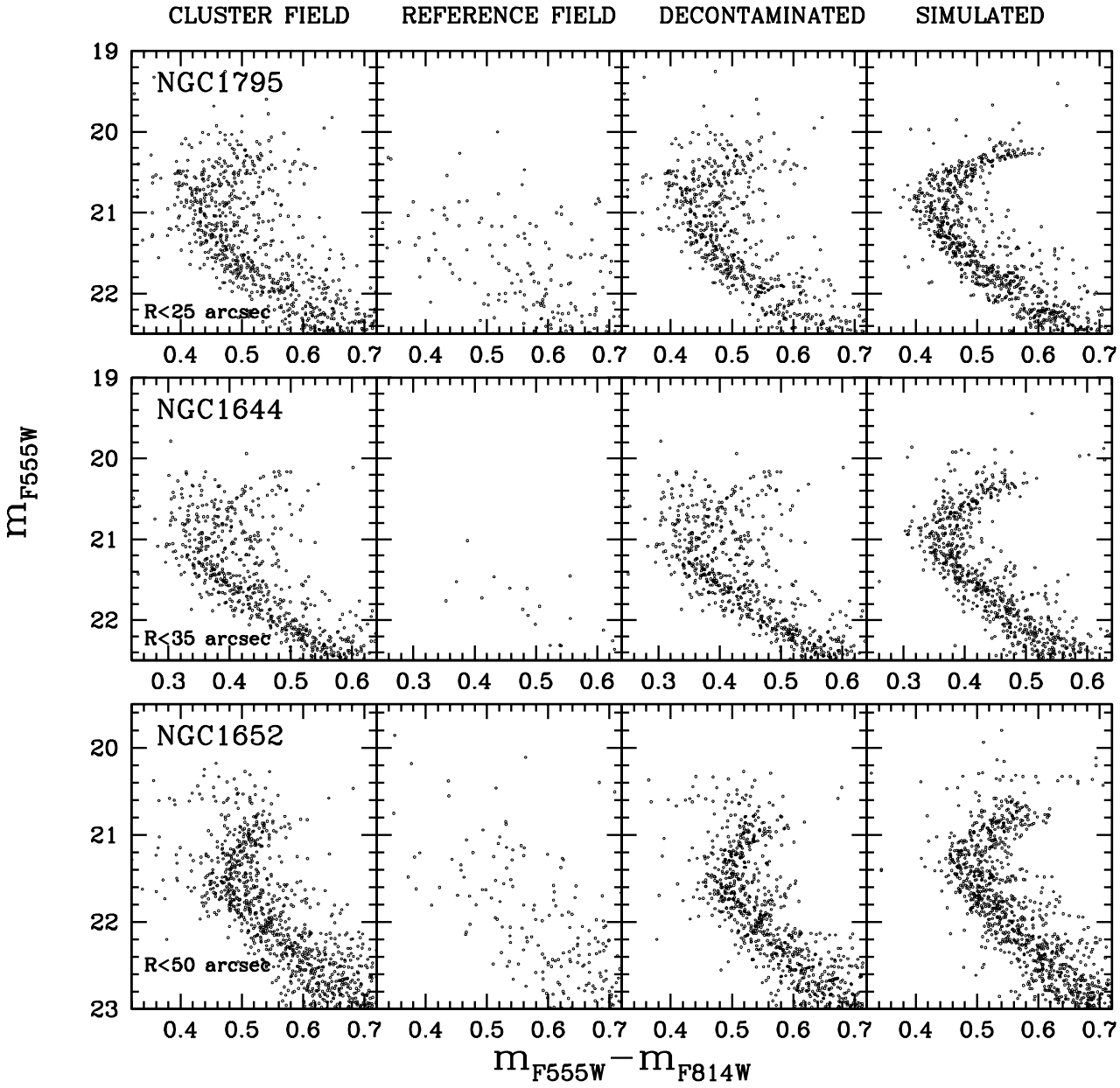

Fig. 35. As in Fig. 31 for NGC 1975, NGC 1644 and NGC 1652.

Milone, A. P., Piotto, G., Bedin, L. R. & Sarajedini, A. 2008, in XXI Century Challenges for Stellar Evolution, Memorie della Societa Astronomica Italiana, vol. 79/2, eds: S. Cassisi, M. Salaris (arXiv:0801.3177)

Mucciarelli, A. Origlia, L., & Ferraro, F. R. 2007, AJ, 134, 1813

Pietrinferni, A., Cassisi, S., Salaris, M., Castelli, F. 2004, ApJ, 612, 168

Pietrinferni, A., Cassisi, S., Salaris, M., Castelli, F. 2006, ApJ, 642, 797

Piotto, G. et al. 2005, ApJ, 621, 777

Piotto, G. et al. 2007, ApJ, 661, L53

Piotto, G. 2008, in XXI Century Challenges for Stellar Evolution, Memorie della Societa Astronomica Italiana, vol. 79/2, eds: S. Cassisi, M. Salaris (arXiv:0801.3175)

Piotto, G. et al. in preparation

Salpeter, E. 1955, ApJ, 121, 161

Sarajedini, A. et al. 2007, AJ, 133, 290

Sollima, A., Ferraro, F. R., Bellazzini, M., Origlia, L., Straniero, O., & Pancino, E. 2007, ApJ, 654, 915

Sirianni, M. et al. 2005, PASP, 117, 1049

Ventura, P., D'Antona, F., Mazzitelli, I., & Gratton, R., 2001, ApJ, 550, 65

Villanova, S. et al. 2007, ApJ, 663, 296

Yong, D., Grundahal, F., Johnson, J. A., & Asplund, M. 2008, (arXiv:0806.0187v1)

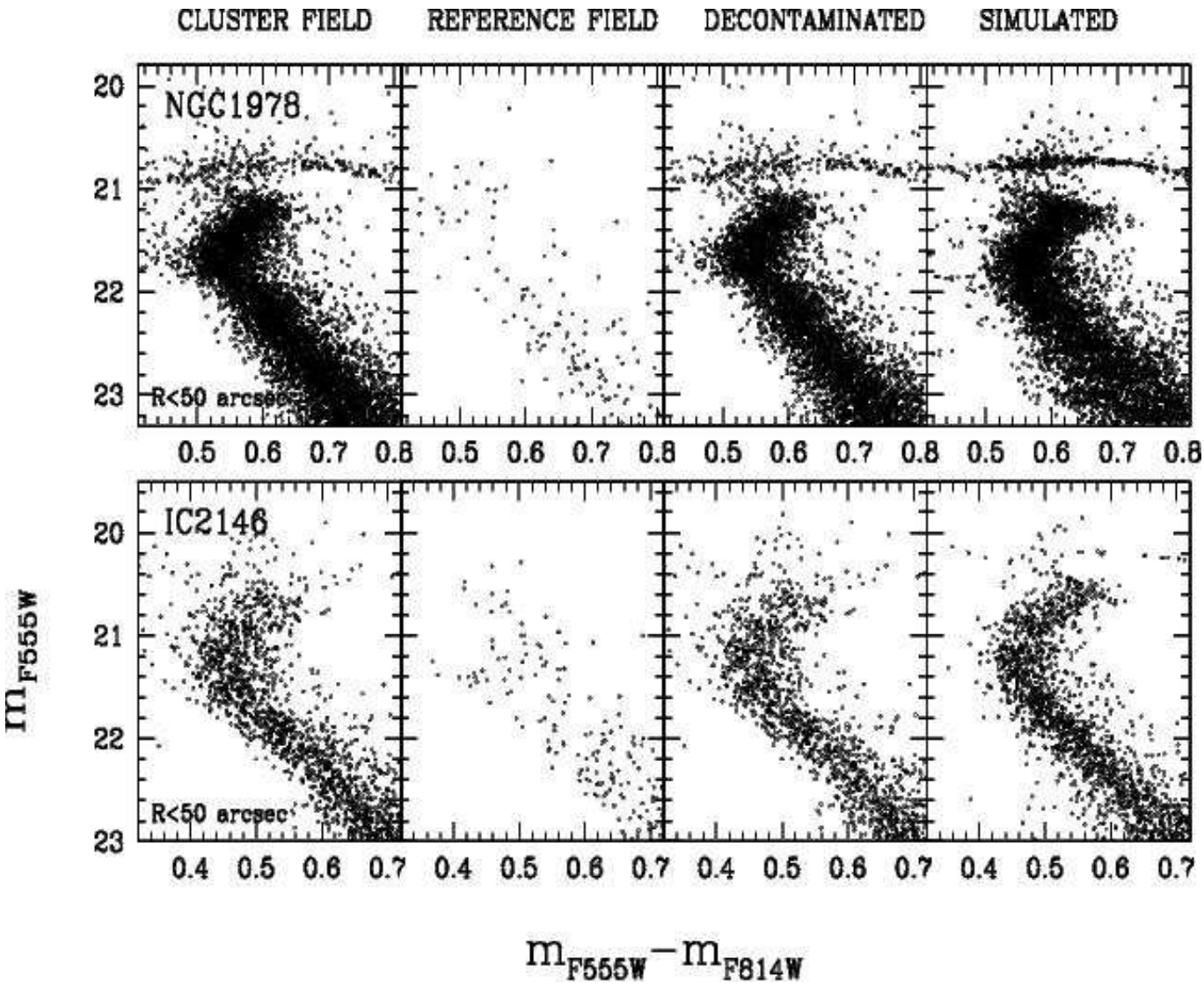

Fig. 36. As in Fig. 31 for NGC 1978 and IC 2146.

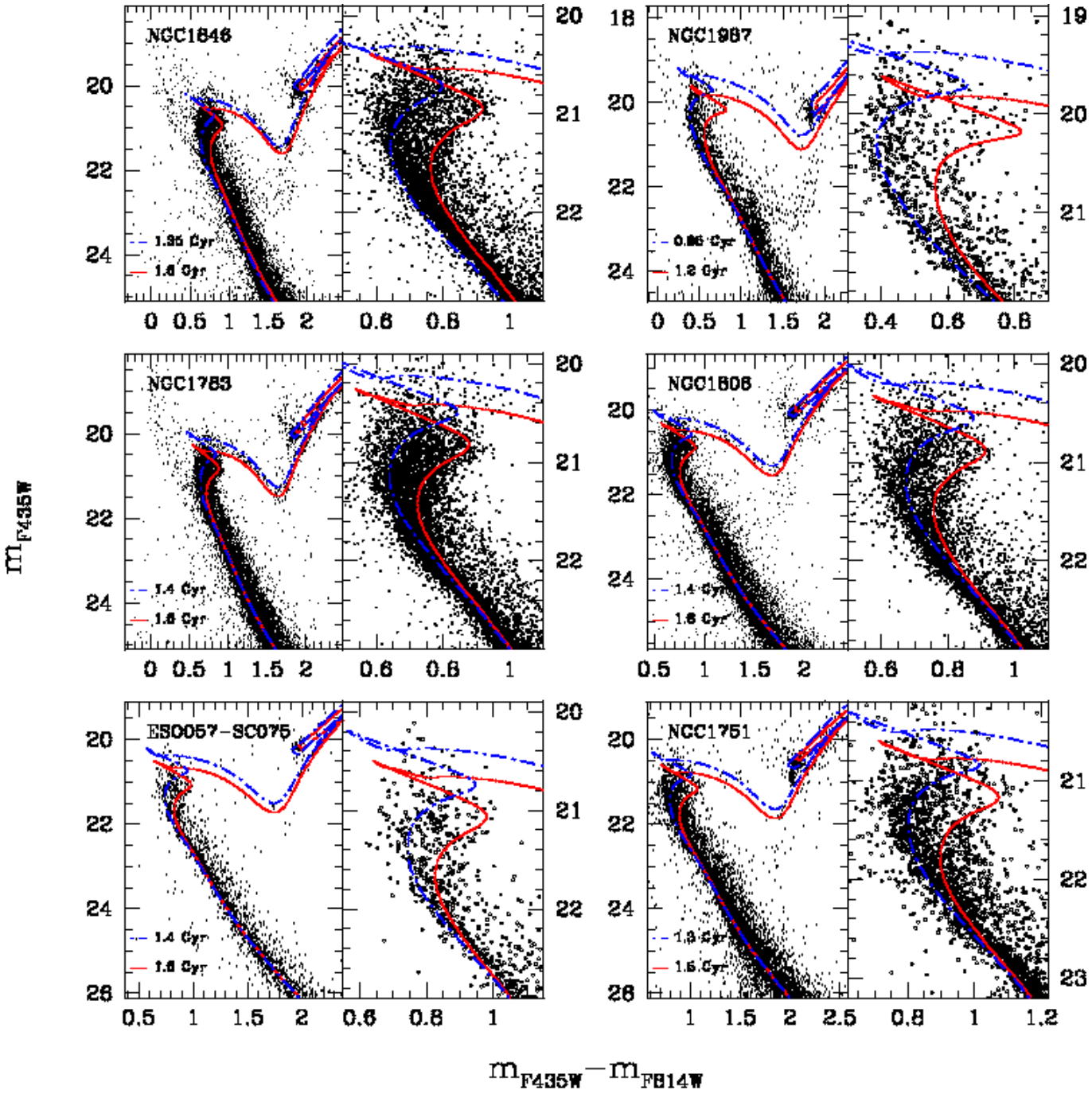

Fig. 37. The best fitting isochrones, obtained by using the distance modulus, reddening, metallicity and age(s) of NGC 1846, NGC 1987, NGC 1783, NGC 1806, ESO057-SC075 and NGC 1751 listed in Table 7 are overplotted to the CMD of the cluster field of (left). A zoom of the region around the MSTO is shown on the right.

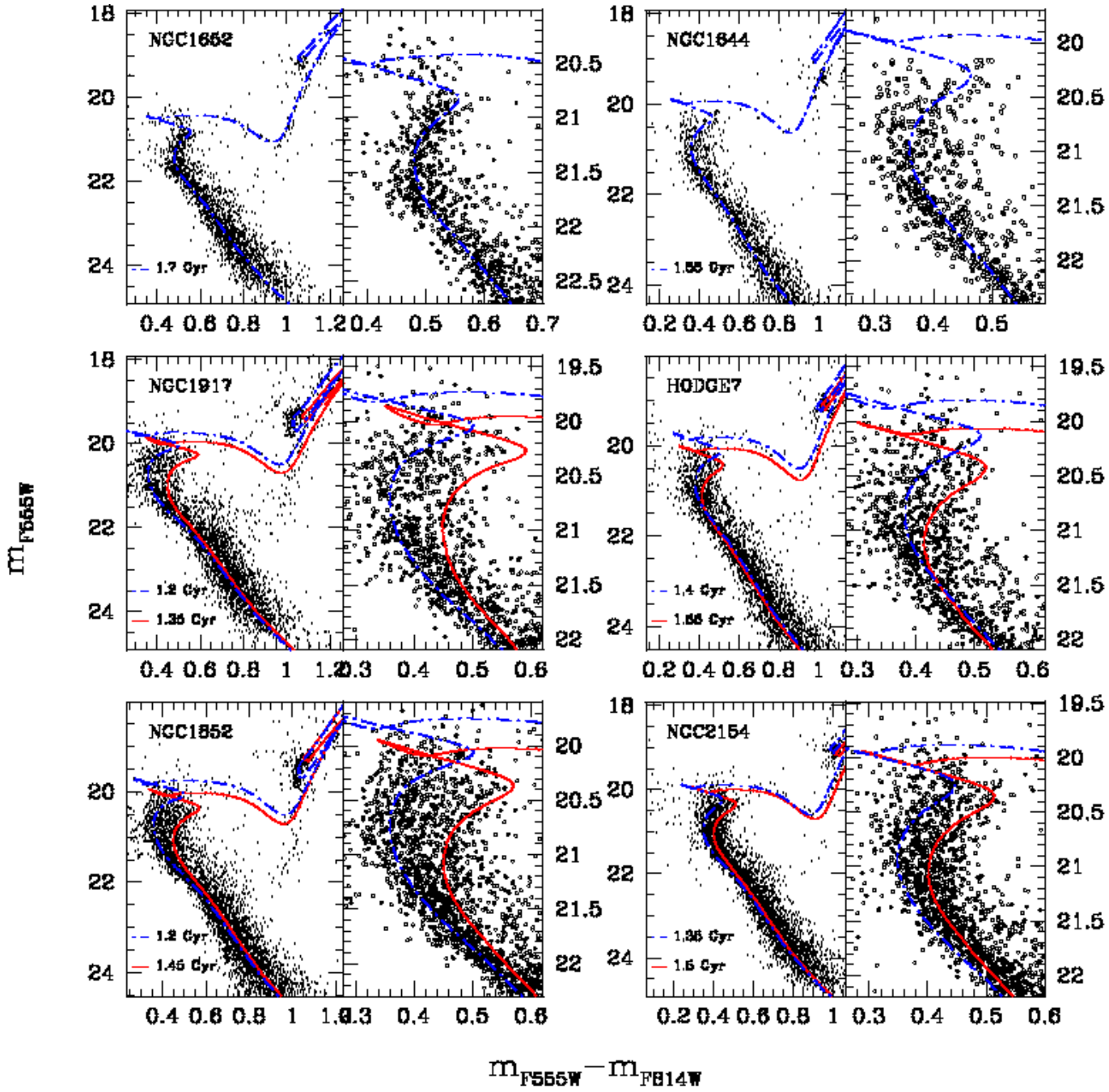

Fig. 38. As in Fig. 37 for NGC 1652, NGC 1644, NGC 1917, HODGE7, NGC 1852 and NGC 2154.

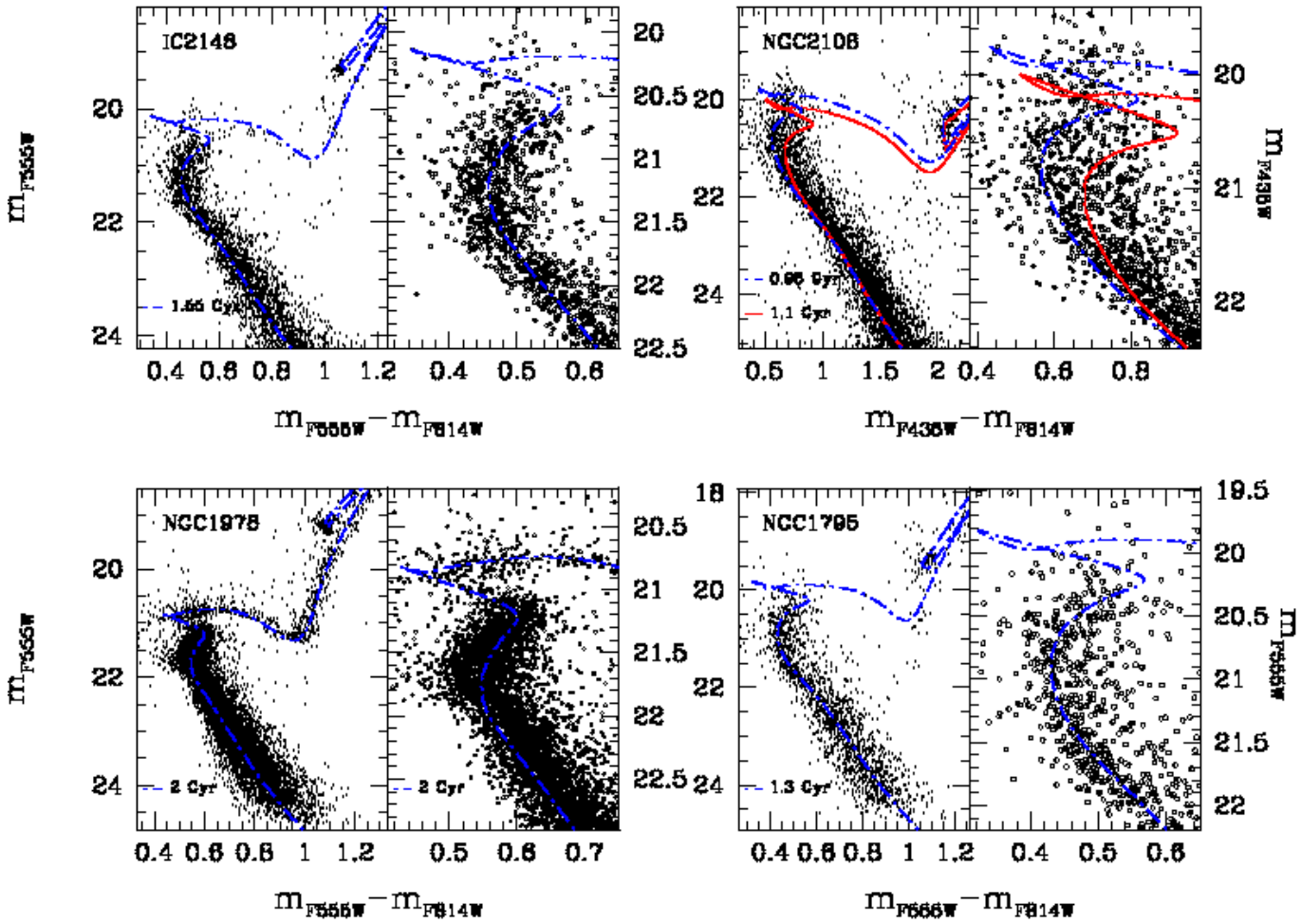

Fig. 39. As in Fig. 37 for IC 2146, NGC 2108, NGC 1978 and NGC 1795.